SYNTHESIS AND CHARACTERIZATION OF INORGANIC FRAMEWORK MATERIALS AND GEL POLYMER ELECTROLYTES FOR LITHIUM-SULFUR BATTERIES

by

Sumeng Chen

Bachelor of Science in Chemical Engineering, Arizona State University, 2016

Submitted to the Graduate Faculty of

Swanson Sschool of Engineeering in partial fulfillment

of the requirements for the degree of

Master of Science in Chemical Engineering

University of Pittsburgh

2018

UNIVERSITY OF PITTSBURGH

SWANSON SCHOOL OF ENGINEERING

This thesis was presented

by

Sumeng Chen

It was defended on

July 26, 2018

and approved by

Prashant N. Kumta, Ph.D, Professor

Department of Bioengineering

Robert Enick, Ph.D, Professor

Department of Chemical and Petroleum Engineering

Hseen Baled, Ph.D, Assistant Professor,

Department of Chemical and Petroleum Engineering

Thesis Advisor: Dr. Prashant N. Kumta, Professor, Department of Bioengineering

SYNTHESIS AND CHARACTERIZATION OF INORGANIC FRAMEWORK MATERIALS AND GEL POLYMER ELECTROLYTES FOR LITHIUM-SULFUR BATTERIES

Sumeng Chen, M.S.

University of Pittsburgh, 2018

Lithium sulfur batteries have been the focus of much attention in recent years due to the high theoretical capacity (~1675 mAh/g) of sulfur as compared to the traditional oxide-based cathode materials. However, sulfur-based cathodes suffer from rapid capacity fade and low charge/discharge capacities due to the formation of soluble polysulfides (PS), consequent PS shuttling and low electronic conductivity of sulfur hindering its transition to commercial lithium ion batteries (LIBs). Inorganic framework materials (IFM) are used in this study as host due to their high temperature stability to contain the PS, reduce the ensuing PS dissolution/transport and accordingly improve the Li conductivity of the sulfur-based cathodes. Sulfur was successfully entrapped into the IFM by employing moderate temperature vacuum infiltration technique and the formation of the IFM-Sulfur (IFM-S) composite was confirmed by XRD, SEM and TEM analysis. The Li-ion conductivity of these IFM-sulfur (Li-IFM-S) composites was further improved by ion exchange methods leading to improvement in the specific capacity with also reducing the fade rate as compared to IFM-S when tested in LIBs using liquid electrolyte. Electrospun composites of PVdF-HFP, polyacrylonitrile (PAN), Bis(trifluoromethane)sulfonimide lithium salt (LiTFSI) and Na/Ti - IFM were used to replace the traditional liquid-based electrolytes and further prevent PS dissolution/shuttling. The electrospun membranes served as suitable host matrices for generating

composite polymer electrolytes (CPEs) activated with 1M LiTFSI, 0.1M $LiNO_3$ in Dioxolane/Dimethoxyethane (50:50 vol.%). The PAN/PVdF-HFP/Na-IFM based CPE with commercial sulfur cathode showed improved performance in LIBs by suppressing PS dissolution, with an initial discharge capacity of 944.74 $mAh \cdot g^{-1}$ at C/8 rate. The combination of Na-IFM incorporated as fillers into CPE membrane as electrolyte, Li-IFM-S as the corresponding sulfur cathode and surface engineered lithium (SE-Li) anode showed improved electrochemical performance in LIB, when compared to commercial sulfur cathode/pristine Li anode/liquid electrolyte system due to entrapment of PS and suppressed PS dissolution/shuttling. The hybrid composite system showed a first cycle discharge capacity of ~925 $mAh \cdot g^{-1}$ at ~ C/14 rate and a very low fade rate of 3.33 $mAh \cdot g^{-1}$ $cycle^{-1}$ (~0.0036 % loss per cycle) at the end of 25 cycles. This high electrochemical performance is the consequence of a combination of novel CPEs and Li-IFM-S. This improved cycling performance demonstrates the promise of Li-IFM-S cathode, PAN + PVdF-HFP with 10 wt. % Na-IFM electrolyte and SE-Li warranting further studies as a high-performance system for high energy density Li-S rechargeable batteries.

Key words: Lithium sulfur battery; composite polymer electrolyte; nanofillers; engineering lithium anode; inorganic framework cathode

TABLE OF CONTENTS

LIST OF TABLES

LIST OF FIGURES

ACKNOWLEDGEMENT

Firstly, I would like to express my great thank to my thesis advisor, Prof. Kumta, for his support, encouragement and valuable suggestion during my master research. I am very appreciative of him giving me the opportunity to work in his energy lab. His knowledge, experience and passion for research always stimulated and gave me the encouragement to keep working on my project no matter how difficult and challenging it appeared to be. He has been teaching me to extend my scientific horizons in energy storage system that makes me get lots of experience on Li-S batteries. Secondly, I would like to thank all my committee members, Dr. Robert Enick and Dr. Hseen Baled, who have offered their valuable advice on my research. Thirdly, I would like to thank all of my colleagues for their continuous help and guidance without whose support it would have been impossible for me to improve my laboratory experience and gain knowledge in batteries. Especially, Pavithra Murugavel guided me with lan instrument and helped me characteritices study of materials. Bharat Gattu taught me on cathode materials. Also, Piyathip Thanapisitikul guided me on surface engineered lithium. Finally, I would like to express my great gratitude to my parents for supporting my study abroad.

1.0 INTRODUCTION

1.1 MOTIVATION

For the existence of human, different kinds of energies are of great necessity. Apart from that, they are important for the development of human civilization. The urgent thing is to make use of energy in an environmental-friendly, sustainable, and effective fashion, in order to satisfy the demands of industrialized nations and meet the needs of the growing global population. In America, over four fifths of energy consumption come from fossil fuel[1]. It is worth mentioning that continuous dependence of fossil fuel will not only exhaust the resources but also give rise to increasing carbon emission. As a result, it will bring about climate change and global warming due to excessive CO_2 generation, an outcome that is direr in nature. Nowadays, more and more energy is utilized from renewable sources such as wind, solar, oceanogenic and geothermal heat. While being continually replenished and hence, indefinite and ethereal in nature, these sources are in general, non-mobile and geographically constrained in their availability, thereby, severely limiting their wide range applicability.

At the same time, electrochemical energy storage devices such as batteries and capacitors, wherein, stored chemical energy is used to generate electricity and fuel cells which convert electrochemical energy to electricity, all offer a pragmatic solution for a wide range of applications such as portable electronics, electric vehicles, grid energy storage including space exploration. A

Ragone plot (**Fig.1**) is typically used to compare the energy and power capabilities of these storage systems. While capacitors are used for high power applications, fuel cells are mainly employed as large energy generation devices. On the other hand, batteries fall in the intermediate range, thereby enabling them to be used for a broader market comprising of portable electronics including the transportation sector largely dominated by plug-in hybrid and all electric vehicles[2].

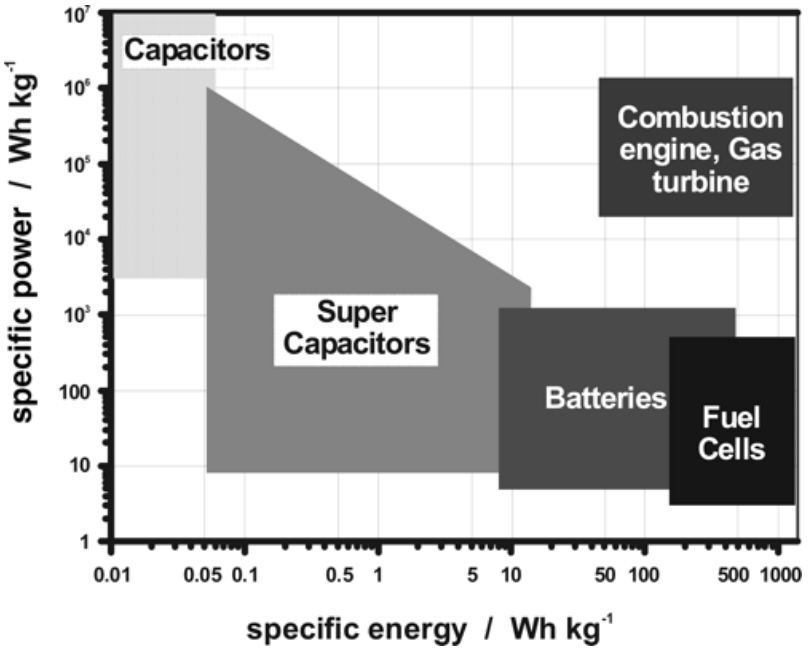

Figure 1. A simplified Ragone plot or diagram showing the energy domains of different electrochemical storage systems compared with the conventional internal combustion gas engine[2]

Among the battery systems, lithium-ion batteries (LIBs) have emerged as the primary energy storage systems for portable energy storage applications since they have not only the high energy density needed but also the flexible design[3]. In 1990, Sony Corporation commercialized the first LIB. Since then, they have been used widely as the energy storage devices for consumer electronics such as cell phones, camcorders, laptops and personal digital assistants (PDAs), digital cameras and their recording and communication media. Over the past decade, plenty of

improvements have been made in terms of storage capacity, long term stability, shelf life and safety, which has consequently contributed to the LIBs entering into the electric tools market and electric vehicle market in the form of EVs (Electric Vehicles) and PHEVs (Plug in Hybrid Electric Vehicles). Admittedly, there are multiple improvements. Meanwhile, the demand for the automotive market continues to grow, and the burgeoning economies of the emerging markets in the world also continue to accelerate. All these developments and incessant demands across the globe continues to propel the impetus for identification and development of cost-effective electrochemically active materials with improved cyclability, rate capabilities and especially high energy and power densities. Although the the first LIB by Sony was commercialized in 1991, current LIBs still employ graphite with a theoretical capacity of 372 mAh/g, as the anode combined with $LiCoO_2$ or $LiMn_2O_4$ as the standard cathode[4]. There is clearly a major need to identify and develop newer systems having much higher energy and power densities.

1.2 LITHIUM-ION BATTERY

A lithium-ion battery can be connected either in series or parallel with a single or multiple electrochemical cell, while lithium (Li^+) ions shuttle between the negative and positive electrodes during charging/ discharging processes. Lithium ion battery still highly dominates the battery market now due to the high specific capacity and overall battery voltage along with other competitive systems being lead acid and primary alkaline (Zn-MnO_2) batteries (**Fig 2**). Before the application and commercialization of rechargeable Li-ion systems, Li^+ primarily exists in the battery industry in the form of primary non-rechargeable batteries. Primary Li batteries were first designed by Matsushita (Li-CF_x, 1973) and Sanyo (Li-MnO_2, 1975)) in the 1970s were mainly

used in artificial cardiac pacemakers, light emitting diode (LED) fishing boats, cameras and in portable memory back-up applications[5]. Recently, these battery systems until in use are mainly comprised of lithium metal anode and are used in direct applications following which they are discarded after all the electrochemical energy is exhausted by the conversion of the chemical energy into electrical energy.

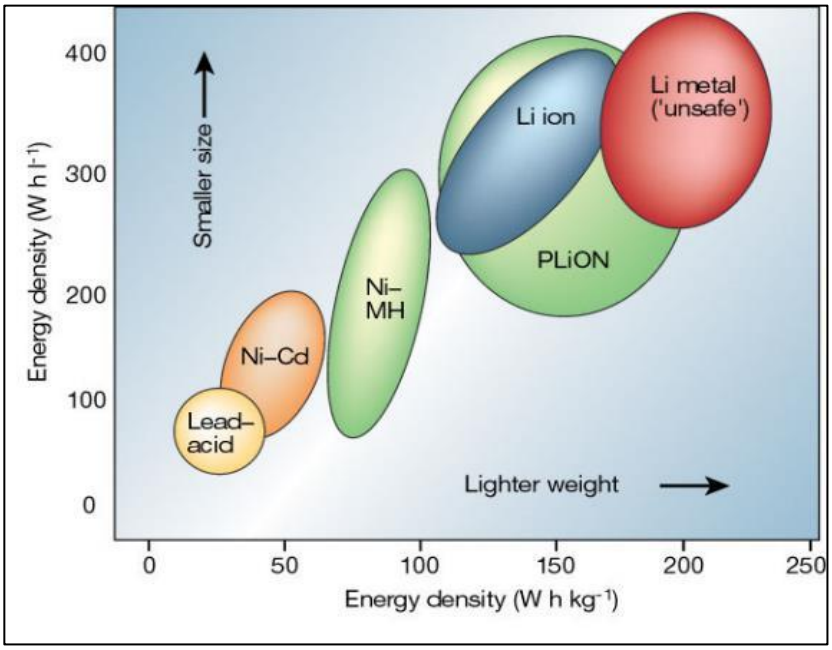

Figure 2. A simplified Ragone plot or diagram showing the gravimetric and volumetric specific energy density domains of different secondary batteries[6]

The first generation of rechargeable lithium-ion batteries made up of Li metal anode and titanium disulfide (TiS_2) as cathode delivering an energy density of 480 Wh/Kg[7]. However, the use of pure Li metal as an anode caused major problems of dendrite formation upon repetitive cycling, which possibly causing short circuit and fire disaster result to safety issues in the battery assembly process[8]. As a result, considerable studies have been conducted to replace the Li metal anode and identify a material that could reversibly store Li in the ionic Li^+ form, substituting the

use of Li metal. This conception triggers the concept of lithium ion battery with the identification of carbon as the host in mid to late 1980's. The research spawned the era of lithium-ion batteries that has being actively explored over past decades[9].

1.3 LITHIUM-SULFUR BATTERIES

1.3.1 Principles of Li-S battery

A Li−S battery is certain electrochemical storage device which can be stored electric energy in sulfur electrodes. A schematic of the components in a single Li−S cell and its charge/discharge process is shown in **Fig. 3**.

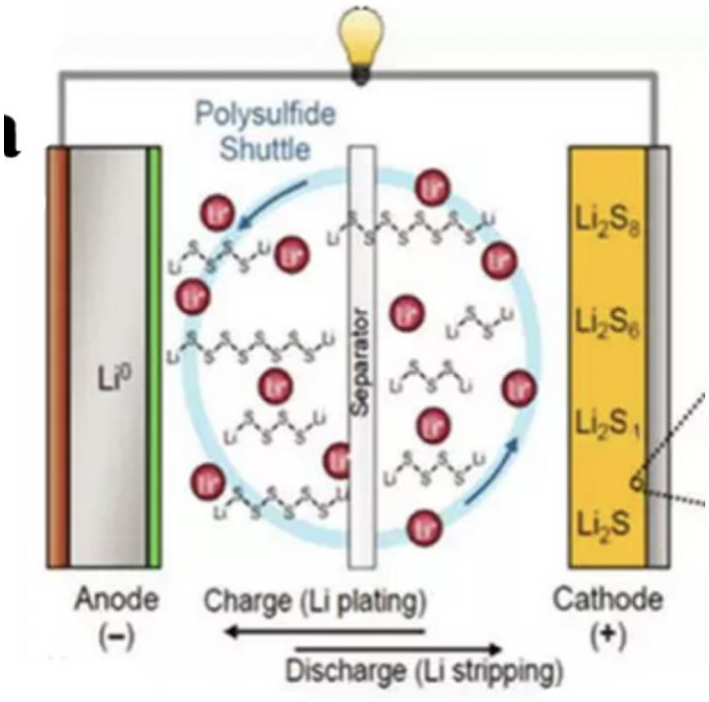

Figure 3. Schematic diagram of a Li−S cell with its charge/discharge operations[10]

A conventional Li−S battery consists of a Li metal anode, an organic electrolyte, and a sulfur composite cathode. Because sulfur is in the charged state, the cell operation starts with discharge. During the discharge reaction, Li metal produces Li-ion and electrons after be oxidized at cathode. The Li ions produced migrate to the positive electrode via the electrolyte internally while the electrons travel to the positive electrode through the external electrical circuit, so that an electrical current is generated. Sulfur is reduced to produce lithium sulfide by accepting the lithium ions and electrons at the positive electrode. The reactions occurring during discharge are given below, and the backward reactions will occur during charge.

Negative electrode: anodic reaction

$$2Li \rightarrow 2Li^{+} + 2e^{-} \quad (1)$$

Positive electrode: cathodic reaction

$$S + 2Li^{+} + 2e^{-} \rightarrow Li_2S \quad (2)$$

Overall cell reaction (discharge)

$$S_8 + 16Li^{+} + 16e^{-} \rightarrow 8Li_2S \quad (3)$$

The theoretical capacities of lithium and sulfur are respectively 3,861 and 1,672 mAh/g, which is nearly five-fold more than the current Li-ion batteries, that leads to a theoretical cell capacity of 1167 mAh/g for the Li−S battery. The average cell voltage of the discharge reaction is 2.15 V. Hence that result to theoretical gravimetric energy density of 2510 Wh/kg for a Li−S cell[11].

Sulfur atoms presents a strong tendency to interlock, forming long homoatomic chains or homocyclic rings of various sizes[12]. Octasulfur (cyclo-S_8), which crystallization is orthorhombic α- S_8 under 25℃ is the most stable allotrope at room temperature. Cyclo-S_8 is reduced and the ring opens during an ideal discharge process, leading to the formation of high-order lithium

polysulfides Li_2S_x ($6 < x \leq 8$). As the discharge continues, lower order lithium polysulfides Li_2Sx ($2 < x \leq 6$) are formed by reacting with the additional of lithium. There are two discharge plateaus at 2.3 and 2.1 V with ether-based liquid electrolytes, which represent the conversions of S_8 to high-order lithium polysulfide and it convert to Li_2S that is the final state of polysulfide. **Fig. 4**[13] is shown the whole process of the formation of polysulfides.

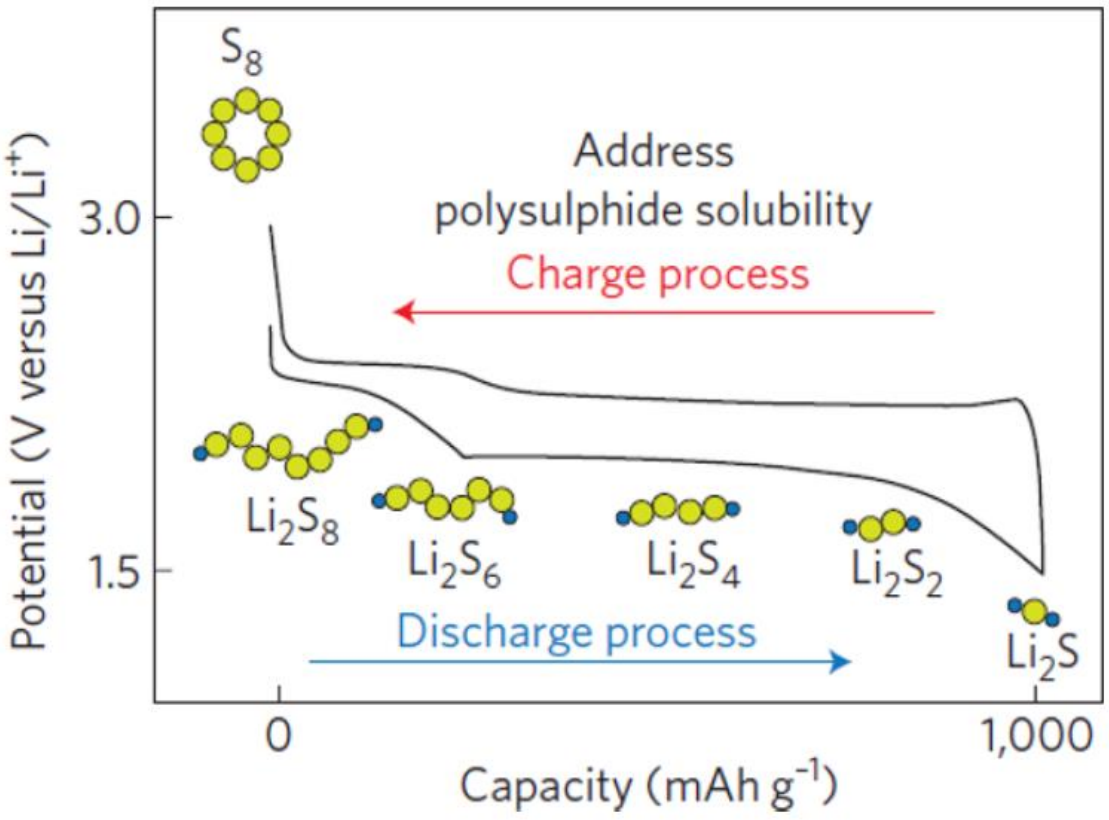

Figure 4 .Voltage profiles of a Li−S cell[13]

During the following charge process, Li_2S is converted to S_8 by forming the intermediate lithium polysulfides, result to a reversible cycle[14-15]. However, the two charge voltage plateaus normally overlap with each other.

1.3.2 Challenges of lithium-surfur battery

Although there are many advantages for the application of Li-S battery, there are still many challenges facing the Li−S technology, either with the materials of electrode or with the system itself. These include:

1. First of all, the high resistance of sulfur ($\sim 10^{-30}$ S/cm) and the intermediate products (i.e., lithium polysulfides Li_2S_x) formed during cycling process along with their structural and morphological changes are insurmountable challenges, causing the unstable electrochemical contact within sulfur electrodes.
2. Additionally, the dissolved polysulfides shuttle between the anode and cathode during cycling, reacting with both the lithium metal anode and the sulfur cathode, which lead to active material lossing[16-17].
3. Moreover, the electrochemical transformation from sulfur to lithium sulfide involves structural and morphological changes as well as repetitive dissolution and deposition of reactive substances, which is trended to passivate both cathode and anode, leading to a significant increment of impedance. These issues result in a low utilization of the active material, poor cycle life, and low system efficiency. Thus, the conventional Li−S battery electrode shown in **Fig. 2** cannot meet all the requirements of Li−S batteries for practical applications.

Consequently, the several problems need to be solved to promote Li−S batteries truly feasible on both technically and commercially way: The shuttling mechanism of polysulfides resulting from the dissolution of the cathode active material must be eliminated to avoid low Coulombic efficiency and the ensuing self-discharge behavior. Also, the amount of carbon additives needs to be reduced as much as possible since too much carbon could reduce the volumetric energy density

of Li−S cells. Full utilization of the sulfur cathode to achieve the full capacity of sulfur (1672 mAh/g) is another challenge because the lower plateau redox reaction is quite slow compared to the upper plateau redox reaction due to slow solid-state diffusion when low-order polysulfides are reduced to Li_2S[16, 18]. In addition, some persistent issues with the lithium metal anode such as dendrite formation and surface passivation still need to be solved. Other alternative anode materials to replace lithium metal might also be an option to be considered due to the safety issue concerns of fire and explosion owing to shorting of the cells and consequent thermal runaway causing the organic electrolytes to catch fire.

1.3.3 Sulfur cathodes

1.3.3.1 Sulfur composite electrodes

The first Li−S cell was designed about 30 years ago. However, the insulating nature of the active material and the polysulfide shuttling effect became critical and chronic technical problems impeding the progress and commercialization of the Li−S technology[10, 19]. Providing a solution to the problem of high cathode resistance is straightforward. This involves identifying an appropriate electrical conductor (conductive carbon/polymer additives) to be added in a well-dispersed form in the active material to ensure good electron transport between the electrically conducting component and the active material. About 10 years ago, conductive carbons and conductive polymers were added to sulfur cathodes to form (i) S−C composites and (ii) sulfur-conductive polymer composites. The conductive carbon was added to S−C composites to enhance the electrical conductivity and active material utilization of the sulfur cathode. For example, the carbon black that is very frequently used for preparing the active material mixture paste has high electrical conductivity to decrease the cathode resistance[20]. Furthermore, the active carbon also has a high

surface area and abundant micropores for infiltrating the active material, which is essential for limiting polysulfide dissolution[11, 15]. On the other hand, identification of sulfur-conductive polymer composites began with the use of polyacrylonitrile (PAN) that showed a high initial discharge capacity of 850 mAh/g[21]. As a result, since then, various types of conductive/porous carbon materials and conductive polymers have been incorporated into sulfur over the past decade[19, 22-24].

1.3.3.2 Porous framework electrodes

Among the conductive additives, porous/conductive carbon has received considerable attention due to its porous structure and higher electrical conductivity compared to that of polymers, which are essential criteria for simultaneously accommodating the active material and enhancing the cathode conductivity[25-26]. The cathode conductivity is increased primarily by following two approaches addressing mainly changes in morphology: (i) formation of a conductive carbon network, e.g., using carbon nanoparticle clusters, and (ii) generating an intimate connection between the conductive framework and the insulating sulfur. Moreover, the engineered porous carbon, mesoporous carbon, and macroporous network not only promotes retention of sulfur but also enhances the charge and electrolyte transport in the composites. Thus far, various carbon materials and synthesis routes that are dedicated to optimizing the composite configuration have provided significant improvements in the cycling performance of Li−S cells.

The mesoporous carbon has been identified as an ordered sulfur encapsulation substrate[27]. After systematically analyzing a series of mesoporous carbon materials with tunable pore sizes and pore volumes, Li et al[27]. indicated that mesoporous carbon with a larger pore size can tolerate a higher maximum sulfur loading and still display good cell performance under full sulfur-filling conditions, which stimulates hopes of improving the currently limited sulfur content/loading in

sulfur-porous carbon (S−PC) composite cathodes. On the other hand, under partial sulfur-filling conditions and surface modification, the encapsulated sulfur has an optimized electrical contact with the mesoporous substrate, which can limit the dissolution/diffusion of polysulfides and ensure a steady supply of lithium ions[28]. For example, a mesoporous carbon (MPC) that possesses a pore size of 22 nm and has 50% sulfur filling in the mesoporous spaces (the theoretical maximum sulfur loading in a composite is 84.7%) provides S− MPC composites exhibiting an initial capacity as high as 1390 mAh/g ultimately resulting in a capacity of 840 mAh/g after 100 cycles.

Engineered hierarchical porous carbon includes bimodal micro/mesoporous carbon or a micro/mesopore-decorated porous carbon framework[1, 22, 29-30]. The first significant achievement was contributed by ordered CMK-3 reported by Ji et al[31]. The high sulfur utilization in this system results from the complete redox reaction, which is stabilized within the nanosized electrochemical reaction chamber of the MPCs. Therefore, the MPC works not only as the electronic conduit but also as the active material stockroom. This success encourages the development of numerous hierarchical porous carbon materials with micro/meso/macropores for improving the cycling performance due to the different beneficial physical/ chemical properties[32]. In hierarchical porous carbon, the micropore is designed for encapsulating/immobilizing the active material, which improves the electrochemical activity and also suppresses the loss of active material. The microporous network serves as the electrolyte pathway to ensure good electrolyte immersion. The mesopore usually serves as an essential supporter for reinforcing the physical properties of the micropore or the macroporous network. Generally, a mesopore with a smaller pore size can work with the micropore to accommodate the active material and trap the dissolved polysulfides, suppressing the severe capacity fade[14]. On the other hand, a mesopore with a larger pore size can facilitate charge transport and cooperate with the microporous network to ensure electrolyte

penetration, resulting in high utilization of sulfur[14]. As a result, the major accomplishment of employing the hierarchical porous carbon is the high cooperation that is possible among the "functional micro/meso/microporous carbons" leading to a functional system trapping the dissolved polysulfide species.

1.3.4 Electrolytes

Electrolytes act as the ion transport pathway between the anode and cathode. Liquid electrolytes are widely used in batteries because of their high ionic conductivity. In Li−S batteries, the electrolyte is critical because the intermediate polysulfides could dissolve in the liquid electrolyte and shuttle between the cathode and anode. The solubility of polysulfides in a liquid electrolyte affects the battery performance. In addition, the passivation caused by the reduction or oxidation of the electrolyte on the electrodes, is also related to the composition of the electrolyte, particularly the additives. A solid-state electrolyte could be a better alternative than a liquid electrolyte in terms of reducing the dissolution and shuttling of polysulfides. However, the low ionic conductivity and interfacial instability associated with most solid-state electrolytes lead to more issues when they are used in Li−S batteries.

Separators used in Li ion batteries are porous polymer films, e.g., expanded polypropylene. They physically separate the anode and cathode but allow ionic movements in the liquid electrolyte that are absorbed into the separators. In Li−S batteries, functional separators that can be ion selective become more promising in reducing the shuttle of polysulfides. In this section, different electrolytes and functional separators are discussed.

1.3.4.1 Polymer electrolytes

Polymer and solid-state electrolytes are more favorable than liquid electrolytes in terms of their capability for reducing the solubility of polysulfides and blocking the shuttling of polysulfides in Li−S batteries. In addition, they could protect the lithium metal anode and minimize dendrite formation, which is beneficial for improving the safety and cycle life of the anode and consequently lead to improved Li−S batteries. However, polymer and solid-state electrolytes usually have low ionic conductivity because of the high viscosity of polymers and high energy barrier for lithium ion transport in solid-state electrolytes. Short-chain polymers such as triethylene glycol dimethyl ether (TEGDME) and polyethylene glycol dimethyl ether (PEGDME) have been widely used in Li−S batteries because of their liquidlike property, which allowed good lithium ion transport. For example, Marmorstein et al.[14] compared three polymer electrolytes, including polyethylene oxide (PEO), poly(ethylene−methylene oxide) (PEMO), and TEGDME. It was found that the cell with TEGDME showed a much lower capacity fade rate than the cell with the other two polymers. Kim et al.[33] studied electrolytes containing $LiCF_3SO_3$ in TEGDME with a sulfur−mesoporous hard carbon spherule composite cathode. The cell exhibited high capacity with excellent retention during cycling. In addition, the cell performed well at low temperatures, delivering a capacity of 500 mAh/g at 0°C over 170 cycles. Shim et al.[34] also compared three solvents with different molecular weights, i.e., triglyme, PEGDME 250 (molecular weight (MW)), and PEGDME 500 (MW). The cells with PEGDME 250 and 500 showed very reversible charge and discharge behaviors with high Coulombic efficiency, while the cell with the triglyme solvent showed low efficiency because of the shuttle of polysulfides, indicating that polymers with high molecular weights can indeed reduce the shuttle effect in Li−S batteries. Long-chain PEO

polymers have been widely used as a major component in polymer electrolytes in Li−S batteries. For example, Shin et al.[35] studied the electrochemical properties and interfacial stability of (PEO)10$LiCF_3SO_3$ composite polymer electrolytes with titanium oxide additive. The addition of titanium oxide increased the ionic conductivity of the composite electrolyte and improved the interfacial stability, thereby improving the electrochemical performance. Hassoun et al.[36] also developed a solid-state Li−S battery employing a PEO-based gel-type polymer membrane containing a PEO/ $LiCF_3SO_3$ polymer matrix with finely dispersed nanosized zirconia and a Li_2S−C composite cathode. A cycle life of 50 cycles and high Coulombic efficiency (99.9%) were obtained at elevated temperatures. Liang et al.[37] studied a PEO18/$Li(CF_3SO_2)_2N$ polymer electrolyte containing 10 wt % SiO_2 with a sulfur−mesoporous carbon sphere composite in Li−S batteries. A discharge capacity of over 800 mAh/g was obtained over 25 cycles at 70 °C. The field of polymer electrolytes thus has a good potential for overcoming the limitations presented by the Li-S battery system.

1.3.5 Research objective and specific aims

The overall objective of this Master of Science thesis is to study and understand the main problems associated with the Li-S battery system and to develop new cathodes and separators to address the problems identified. The primary problems of Li-S battery as mentioned above, are the poor electronic and ionic conductivity of sulfur and the formation combined with dissolution of the polysulfide in organic battery electrolyte.

In order to address the poor conductivity of sulfur, conducting zeolite socony mobil-5 (ZSM-5) hosts will be developed for encapsulating sulfur. To overcome polysulfide dissolution, agents capable of trapping the polysulfide will also be developed. Composite polymer electrolytes

(CPEs) and oxides with improved room temperature lithium ionic conductivity will also be developed and their ability to prevent polysulfide dissolution will be studied using materials characterization combined with appropriate electrochemical characterization techniques.

To accomplish the above goals, the broad objectives of this research proposal will comprise executing the following four specific aims:

Specific aim 1: Develop sulfur infiltrated ZSM-5 cathodes to prevent and/or hinder polysulfides from dissolving into the liquid electrolyte.

As a part of this specific aim, ZSM-5 will infiltrated with sulfur using a vapor infiltration technique. The sulfur infiltrated ZSM-5 will be used as cathodes for Li-S batteries. The specific capacity and the cycling stability of the ZSM-S will be evaluated using electrochemical testing.

Specific aim 2: Investigate the mechanisms of composite polymer electrolytes (CPEs) to prevent polysulfide dissolution in Li-S batteries.

In this aim, poly (vinylidene fluoride – co – hexafluoro propylene) (PVdF – HFP) and Polyacrylonitrile (PAN) based CPEs (Composite Polymer Electrolytes) will be prepared by a simple electrospinning technique. Further, commercially available Na-ZSM and Ti-ZSM will be used as fillers to augment the mechanical and Li-ion conducting properties of these CPEs among other necessary ionic transport requirements. These nanofiller incorporated composite polymer electrolytes as separator – electrolytes will then be tested to demonstrate their improved cycling stability using commercial sulfur as cathodes in Li – S batteries.

2.0 EXPERMENTS

2.1 MATERIALS

The polymer Poly (vinylidene fluoride–co–hexafluoropropylene) (PVdF–HFP) (Mw ~400,000, Aldrich), Polyacrylonitrile (PAN) (Mw ~150,000, Aldrich), solvents N, N-Dimethylformamide (DMF) (ACS reagent, ≥99.8%, Aldrich), Acetone (ACS reagent, ≥99.5%, Aldrich) and lithium salt, Bis(trifluoromethane)sulfonimide lithium salt (LiTFSI) (99.95% trace metals basis, Aldrich) used for the electrospinning process were vacuum dried for 12 h at 60ºC before further use.

Commercially available H-ZSM, Na-ZSM and Ti-ZSM (ACS material) was used as-received in this work without any further treatment. Finally, Milli-Q water (18.2 Ω) was used throughout the entire experiment.

2.2 SYNTHESIS OF SULFUR – ZSM5 NANOCOMPOSITES

Commercial H^+ – ZSM – 5 (indicated as HZSM, P-25, SiO_2/Al_2O_3 ~25, 2-5μ particle size, ACS Material) was mixed with commercial sulfur powder (HZSM : Sulfur=85 : 15 weight ratio) and ground in mortar pestle for 15min. Subsequently, the composite powder was loaded into a quartz ampoule which was then evacuated for 10mins and refilled with Argon. The evacuation – refilling process was repeated 5 times after which the quartz ampoule was sealed under vacuum using an oxy acetylene blow torch. This sealed quartz ampoule was then heat treated at 500ºC (1ºC/min

heating and cooling rate) for 18h in a box furnace in a vertical position after which the tip of the ampoule was broken and the sulfur infiltrated powder (HZSM-S) was collected. The H^+ in this sulfur infiltrated HZSM was then ion exchanged with Li^+ by adding 1g of HZSM-S in 100ml of 2M LiCl solution, evacuating the mixture for 15mins and then stirring it at 50ºC for 8h. Subsequently, the Li^+ substituted HZSM-S (hereby indicated as LiZSM-S) was collected by centrifugation and drying in vacuum at room temperature.

2.3 PREPARATION OF PVDF-HFP NANOFIBER MEMBRANE

The composite polymer electrolytes, CPEs of PVdF – HFP: PAN (50:50 w%) and LiTFSI (0.1 w%) were prepared by dissolving the components in a mixed solvent of DMF/acetone (7:3, w/w) at 50ºC for 12 h until a homogeneous solution was formed. The resulting solution was dispersed with **10 wt%** nano – filler (Na-ZSM/Ti-ZSM) under sonication for 12 h. The CPEs were prepared by a typical electrospinning method at room temperature. Electrospinning of the nano – filler dispersed solution was performed at a flowrate of 1 ml/h and a high voltage of 20 kV at room temperature with 15 cm distance maintained between the tip of the syringe and the rotating drum. The nanofibers deposited onto the rotating drum were then collected, dried under vacuum for 12 h at 60 ºC at 1 atm. The nanofiber mats were then heat pressed at 80ºC for 30 min at 1 atm. pressure and activated by soaking in 1.8 M LiTFSI and 1 M $LiNO_3$ in 1:1 vol% Dioxolane/Dimethoxy ethane for 30 min before use as separator – electrolyte complex in Li – S battery.

2.4 SURFACE ENGINEERING OF LITHIUM

Surface engineered lithium was prepared by placing the lithium foil on top of a commercially obtained filer with ridges. The lithium surface was then imprinted by rolling a glass surface (rinsed with acetone) over the lithium to replicate the structure of the ridges on the metallic filer. Similarly, plain lithium anode was prepared by rolling the lithium foil using a clean glass surface to flatten it to approximately similar thickness to that of THE surface engineered lithium. After the surface engineering process, the lithium foil was cut into circular shape, 12 mm in diameter to be used as tue counter/reference electrodes during electrochemical testing. All the electrodes were handled and processed in the MBraun glove box with moisture and oxygen control (O_2, H_2O<0.1 ppm).

2.5 MATERIALS CHARACTERIZATION AND ELECTROCHEMICAL MEASUREMENTS

It is important to understand the nature of the LiZSM-S active composite material, nanoparticulate fillers and the electrospun CPE membranes to explain the observed cycling stability. Accordingly, to investigate the morphology and composition of the HZSM, HZSM-S, LiZSM-S, nanofillers (Na-ZSM, Ti-ZSM) and electrospun CPE membranes, scanning electron microscopy (SEM) analysis was conducted on a Philips XL30 machine operating at 20 kV. The crystal structure of the Na-ZSM/Ti-ZSM nanoparticles and the evolution of ZSM based sulfur composites (commercial sulfur, HZSM, HZSM-S, LiZSM-S) were characterized by X- ray diffraction using Philips XPERT PRO system employing CuKα (λ = 0.15406 nm). The scans were recorded in 2θ range of 10° - 90°, at a constant current of 40 mA and voltage of 45 kV. The nature of chemical

bonding in the CPEs were further analyzed by attenuated total reflectance Fourier transform infrared spectroscopy (ATR-FTIR, Nicolet 6700 spectrophotometer, Thermo Electron Corporation) using a diamond ATR Smart orbit. Spectra were obtained at 1 cm^{-1} resolution averaging 64 scans in the 400–4000 cm^{-1} frequency range. The pore characteristics and specific surface area (SSA) of the nano filler samples were analyzed on a Micromeritics ASAP 2020 Physisorption analyzer, using the Brunauer–Emmett–Teller (BET) isotherm generated. The powders were first vacuum degassed and then tested for Nitrogen adsorption and desorption for the specific surface area analysis.

2.6 ELECTROCHEMICAL CHARACTERIZATION

Electrodes for battery half-cell characterization were prepared by slurry casting 60 wt. % of active sulfur material (commercial sulfur, HZSM-S, LiZSM-S), 30 wt. % acetylene black and 10 wt. % PVdF in N- Methyl Pyrrolidone (NMP) onto aluminum foil followed by drying under vacuum for 24 h. Electrodes with uniform sulfur loading (1.5 mg – 2 mg cm/cm^2) obtained by slurry coating were utilized for all the electrochemical measurements by assembling the electrodes in CR2025 coin cells in Innovative, Inc. inert argon atmosphere glove box (O_2, H_2O<0.1 ppm). Accordingly, sulfur based composite electrodes formed the working electrode, lithium foil as the counter electrode, and the electrospun CPE membranes soaked in liquid electrolyte (1:1 vol% 1, 3 dioxolane and 1, 2 dimethoxyethane with 1.8 M LiTFSI (Bis(trifluoromethane)sulfonamide lithium salt) and 0.1 M $LiNO_3$) as the electrolyte/separator complex. For the initial electrochemical study of sulfur infiltrated ZSM-5 (HZSM-S and LiZSM-S) above mentioned liquid electrolyte was used using Celgard separator instead of CPE membranes in a flooded CR2025 coincell. The

electrolyte to sulfur (E/S) ratio used in the CPE membranes was between 3:1 and 4:1 ml g^{-1}. Control samples were prepared under identical conditions replacing the CPE with 100 µl liquid electrolyte and Celgard 2400 polypropylene (PP) membrane as the separator. The E/S ratio in the control samples was maintained between 50:1 to 65:1 ml g^{-1}. The electrochemical cycling behavior of the cells thus prepared was studied by cycling between 1.7 – 2.6 V (w.r.t. Li^+/Li) at different charge discharge rates (50 mA/g, 100mA/g, etc) using an Arbin BT200 battery testing system with a rest time of 60s between each charge / discharge cycle.

3.0 RESULTS AND DISCUSSION

3.1 MORPHOLOGY STUDY OF INORGANIC FRAMEWORKS

3.1.1 SEM analysis of inorganic frameworks

The morphology evolution/change of inorganic framework material (HZSM-5) and sulfur infiltrated inorganic framework material (HZSM-S) was studied by scanning electron microscopy (**Fig. 5**). The SEM analysis of ZSM-5 (**Fig. 5a, 5b)** shows the presence of agglomerates of particles with an average particle size of ~1-2 µm which is consistent with the commercial specifications. SEM of the HZSM-S (**Fig. 5c, 5d)** indicates no change in the morphology as compared to the commercial HZSM-5 (**Fig. 5a, 5b)** without any formation of discrete sulfur particles. The apparent particle size of the HZSM-S is still less than 1 µm which confirms the successful infiltration of sulfur without any agglomerates formed by the molten sulfur during cooling due to higher weight percentage of sulfur utilized.

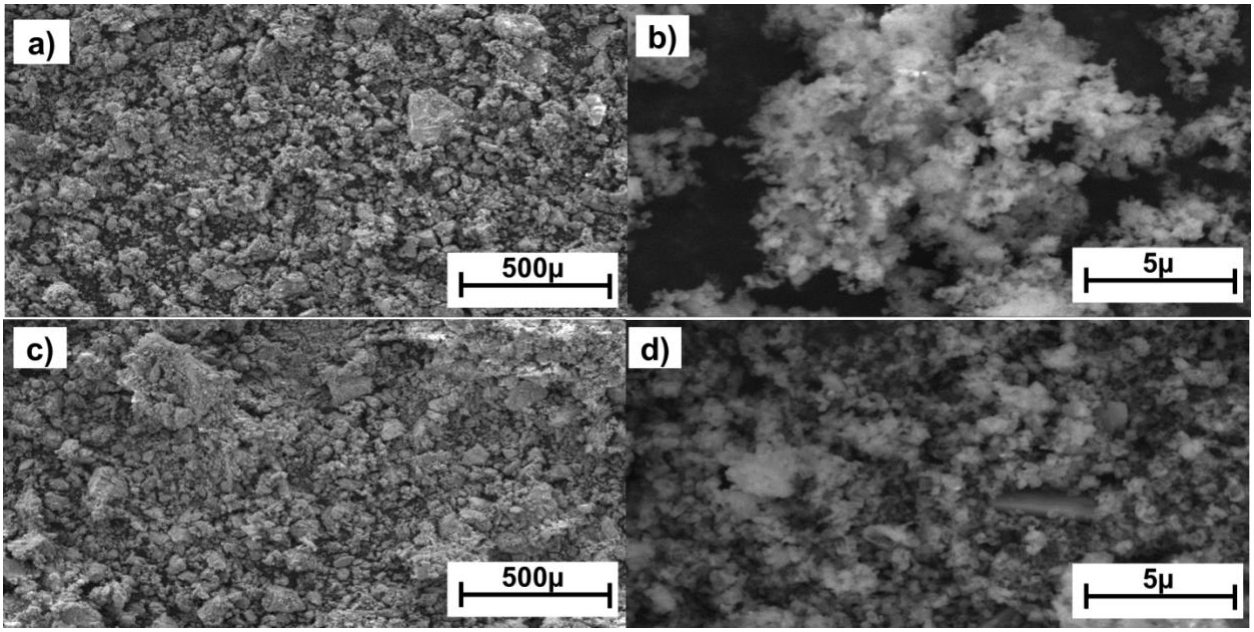

Figure 5. Low and high magnification SEM images of a), b) HZSM-5 and c), d) HZSM-S after sulfur infiltration, respectively.

3.1.2 XRD analysis of inorganic frameworks

The X-ray diffraction spectroscopy (XRD) analysis was performed to confirm the infiltration of sulfur in ZSM-5 the results of which are shown in **Fig.6**. The XRD pattern corresponding to commercial sulfur shows all the crystalline peaks of orthorhombic phase of sulfur (JCPDS card No. 08-0247) while that of HZSM-5 shows the crystalline characteristic diffraction peaks (2θ ~ 7.9º, 8.8º, 14.8º, 23.2º, 23.9º and 24.4°) corresponding to the structure of MFI zeolite (JCPDS card No. 49-0657). Sulfur infiltrated ZSM-5 (ZSM-S), on the other hand shows peaks corresponding to sulfur and HZSM-5 indicating the presence of discrete sulfur inside HZSM-5 without any reaction between sulfur and HZSM-5 during the infiltration process forming a composite structure.

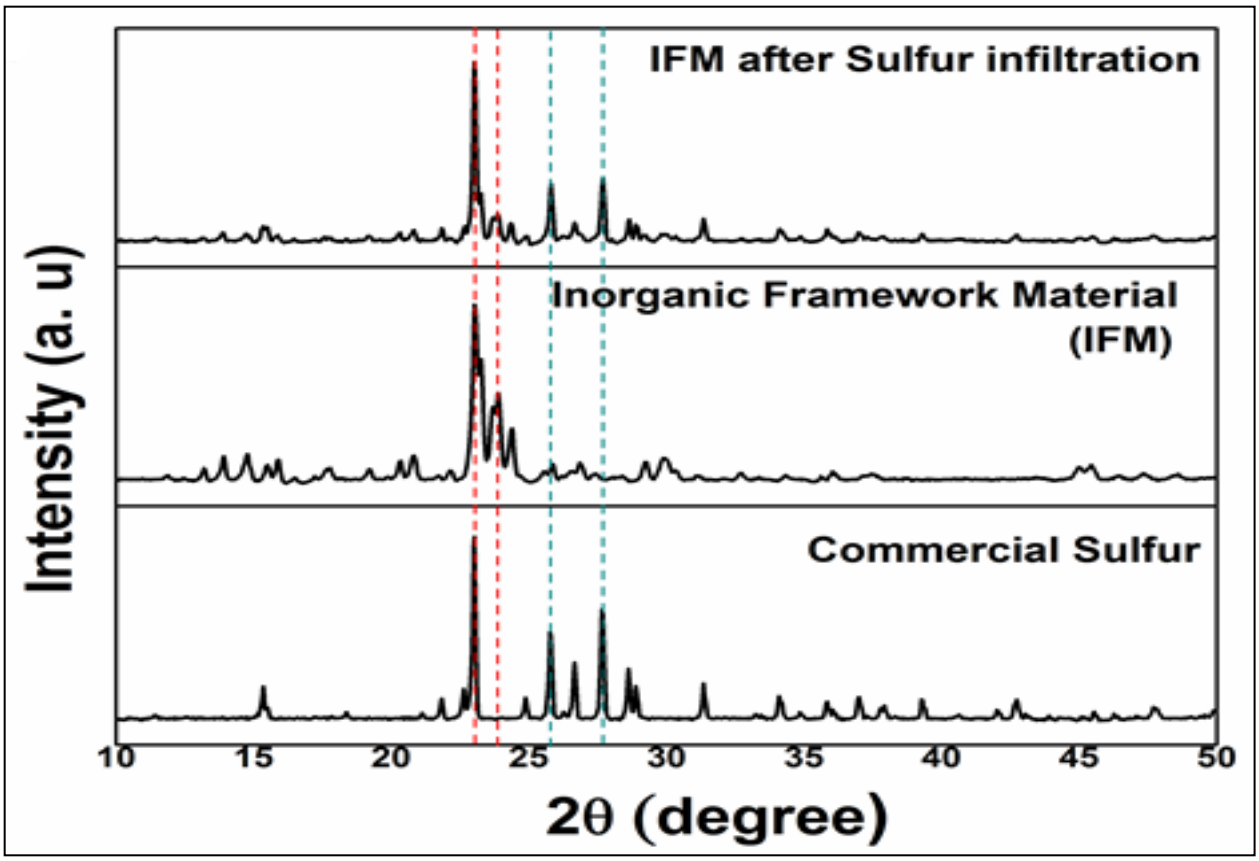

Figure 6. XRD pattern of commercial sulfur (bottom), HZSM-5 (center) and sulfur infiltrated HZSM-5, HZSM-S (Top).

3.1.3 TEM analysis of inorganic frameworks

Transmission electron microscopy (TEM) images of the ZSM-5 zeolites at different magnification are shown in **Figure 7a and Figure 7b**. The TEM indicates rectangular or rhombic morphology of the commercial HZSM-5 zeolite with particle size of ~ 500 nm which is in accordance to the SEM results and concord to the observations of Guo et al. that confirmed the crystal structure and size of commercial ZSM[38]. A high-resolution transmission electron microscopy (HRTEM) image of commercial HZSM-5 (**Figure 7c)** zeolite structure shows crystallographic pores similar to those presented by Zhang et al.[39] that can trap the polysulfides during the discharge/charge process in

lithium-sulfur battery. Additionally, the pores structure provides enough space for volume expansion that occurs during the reaction of sulfur with lithium.

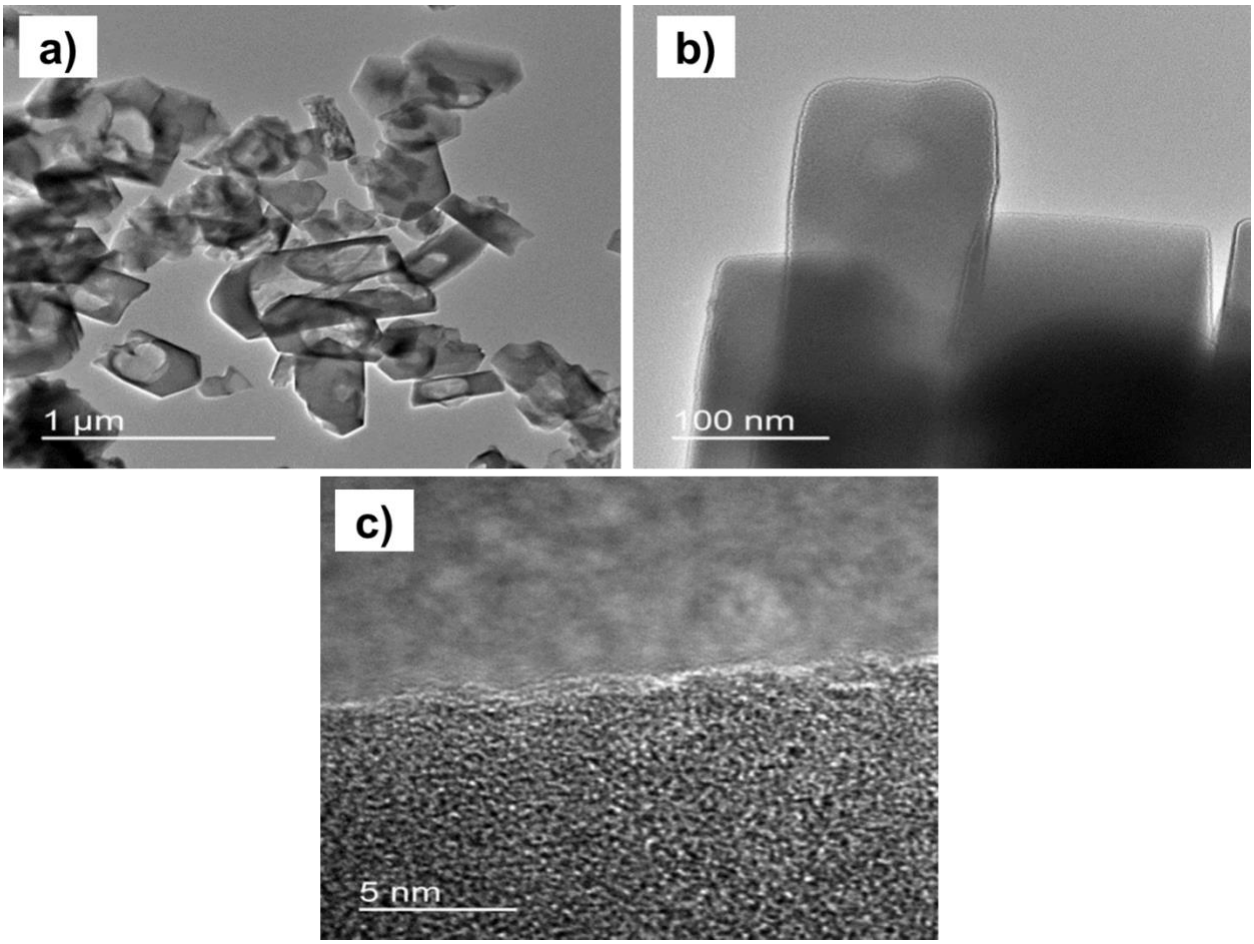

Figure 7. a) Low magnification, b) high magnification and, c) high resolution TEM images of commercial HZSM.

TEM images of HZSM-S shown in **Fig. 8a, 8b** shows the structure of the composite material formed after infiltration of sulfur into the commercial HZSM-5. There is no major change in the particle size of HZSM-S which still remains around 500 nm and the morphology of the commercial ZSM-5 is retained after sulfur infiltration. The HRTEM images shown in **Figure 8c** confirms the presence of islands of sulfur infiltrated into the pores of ZSM-5 and the formation of

this structure after sulfur infiltration into HZSM-5 is expected to trap the polysulfides and hinder the dissolution of the polysulfide species into the electrolyte.

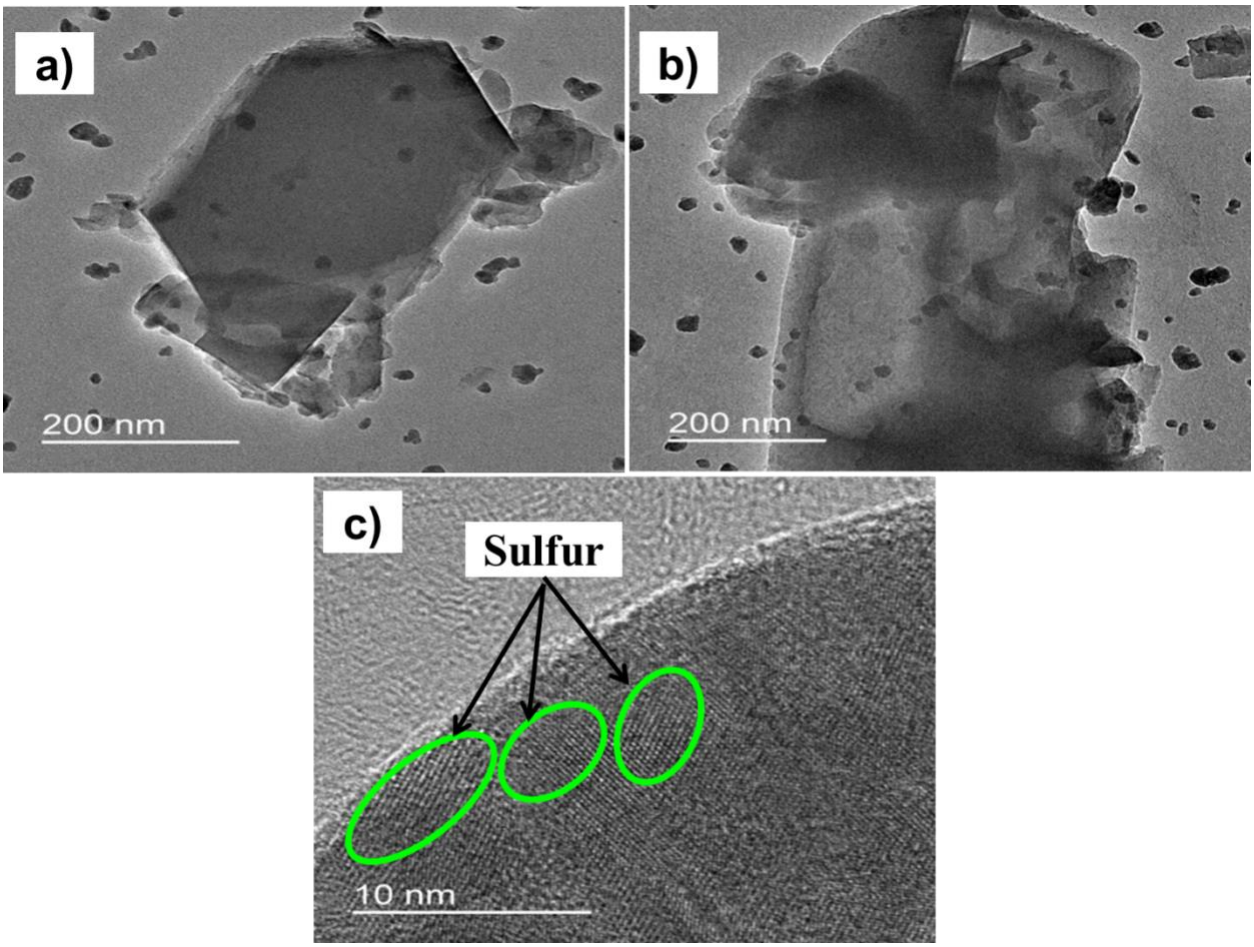

Figure 8. a), b) TEM images of sulfur infiltrated HZSM-5 (HZSM-S) and c) HRTEM image of HZSM-S showing islands of sulfur distributed in the crystallographic pores of HZSM-5 after sulfur infiltration.

3.2 MORPHOLOGY STUDY OF COMPOSITE POLYMER ELECTROLYTES

3.2.1 Specific surface area analysis

Specific surface area of the nanofillers is an important factor deciding the electrochemical performance of the CPEs. It has been observed that smaller size particles for a similar volume fraction of the ceramic filler phase would impart an improved performance as compared to larger size particles because of their ability to cover more surface area[40]. The BET surface area analysis of the nanofillers is presented in **Table 1** which is in accordance with the data sheet provided by manufacturer. The BET surface area analysis has been conducted once to verify the properties with the data provided by manufacturer and additional measurement will be done as a part of future work.

Table 1. BET surface area analsys of Na-ZSM and Ti-ZSM.

	BET Surface Area/ m^2g^{-1}	**Langmuir Surface Area/ m^2g^{-1}**	**Total Pore Volume/ cm^3g^{-1}**	**Adsorption average pore width/ nm**	**BET Surface Area/ m^2g^{-1} (literature)**
Na-ZSM	266.09	425.84	0.160	24.01	330-380[41]
Ti-ZSM	347.82	566.93	0.253	29.08	334-447[42]

The BET surface area results indicate that Na-ZSM has a high BET surface area of 266.09 m^2/g which is closer to the value (330-380m^2/g) from the literatures[41]. Na-ZSM also exhibits a high pore volume of 0.160 cm^3/g. On the other hand, the Ti-ZSM showed a surface area of 347.82 m^2/g. The very high surface area of the Na-ZSM and Ti-ZSM is expected to improve the performance of CPEs.

3.2.2 XRD analysis of gel polymer electrolytes

The CPEs were extensively studied by using XRD analysis. The results of the XRD analysis are shown in **Fig. 9 and Fig. 10**. The Na-ZSM exhibits the major peak at $2\theta = 23.1°$. This peak is retained in the XRD patterns corresponding to the electrospun PVdF-HFP+Na-ZSM, PAN+Na-ZSM and PVdF-HFP+PAN+Na-ZSM. The XRD patterns of the electrospun polymer members also exhibits their characteristic XRD peaks in addition to the peak corresponding to Na-ZSM. The XRD pattern of PAN shows peak at $2\theta = 17.0°$ and PVdF-HFP shows peak at 20.4° which is similar to the results of Jung K.N. et al[43]. The other three peaks at $2\theta = 43.7°$, 51.1°, and 72.8° are due to the LiTFSI.

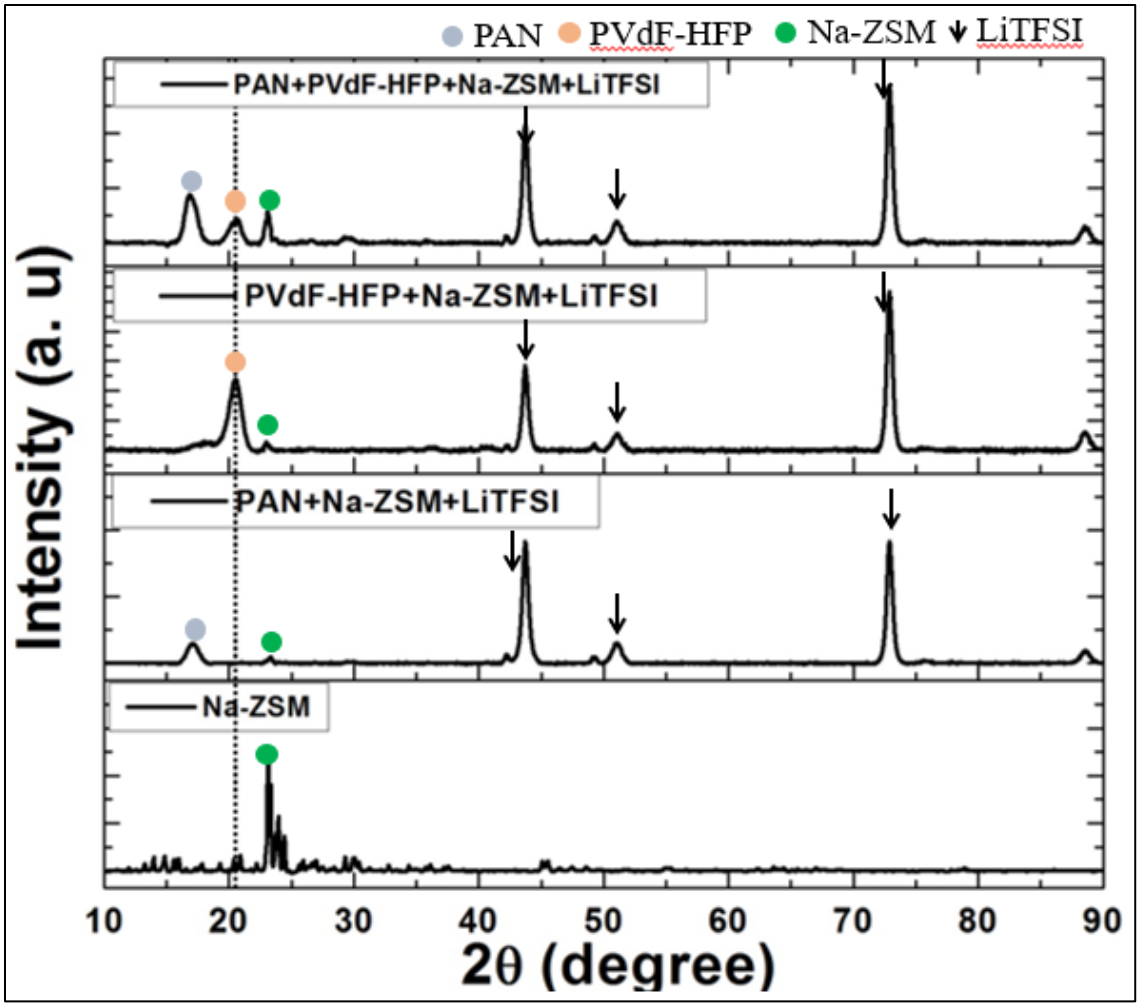

Figure 9. X-Ray diffraction pattern of commercial Na-ZSM; PAN + Na-ZSM + LiTFSI; PVdF-HFP + Na-ZSM + LiTFSI and PAN+ PVdF-HFP + Na-ZSM + LiTFSI indicating the evolution of different phases during synthesis of CPE membranes.

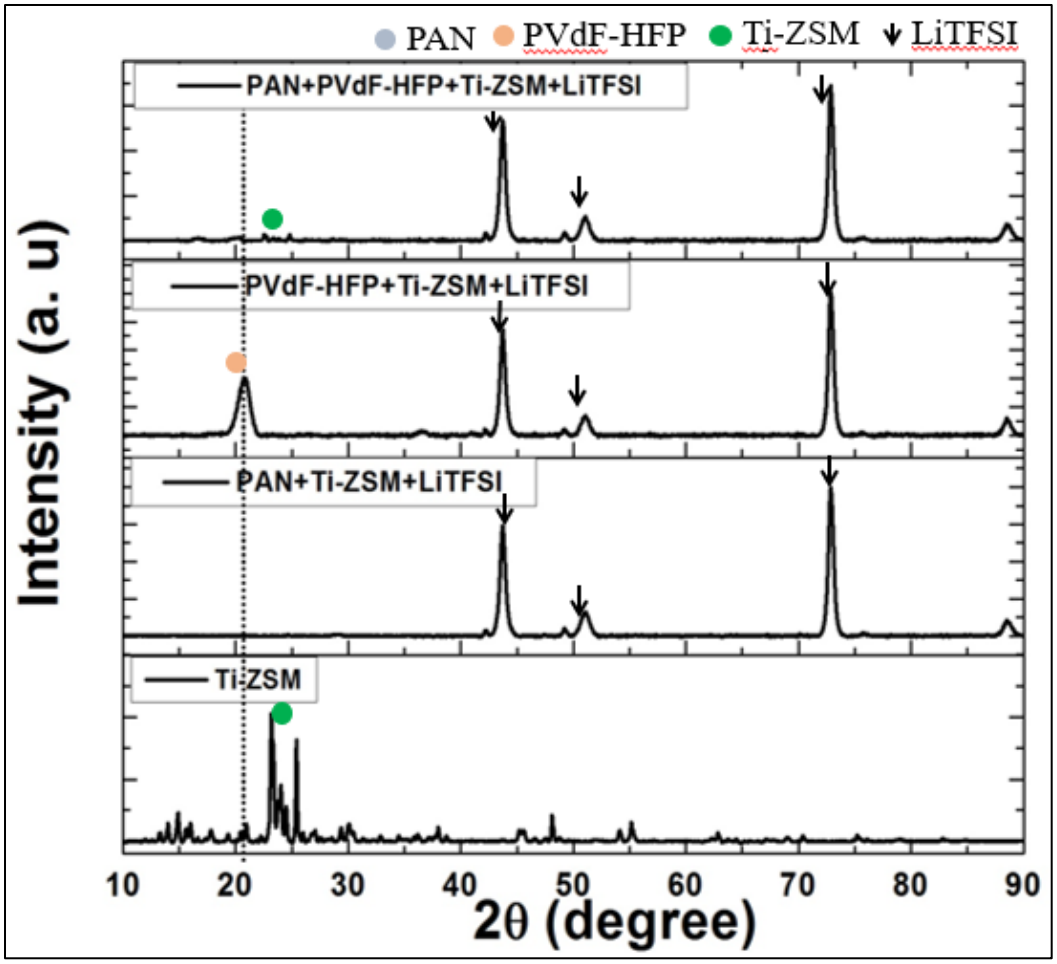

Figure 10. XRD pattern of commercial Ti-ZSM (bottom), PAN + Ti-ZSM + LiTFSI (center) and PVdF-HFP + Ti-ZSM + LiTFSI, PAN+ PVdF-HFP + Ti-ZSM + LiTFS (Top).

3.2.3 FTIR analysis of gel polymer electrolytes

The nature of the chemical bonding between Na-ZSM and PAN, PVdF-HFP and LiFTSI was analyzed using FTIR spectroscopy. In the FT-IR spectra of pure Na-ZSM, peaks are observed at ~1210 - 1220 cm^{-1} and ~1045 - 1070 cm^{-1} which represent the asymmetric stretching of the siloxane groups while the band at ~780 – 795 cm^{-1} represents the symmetric stretching of the siloxane groups of the Na-ZSM. The band of 543 cm^{-1} indicates the internal flexions of the tetrahedrons in the ZSM-5 structure[44].

Addition of LiTFSI to the PVdF-HFP+Na-ZSM shows distinct peaks at 839, 847 and 1491 in the FTIR spectra corresponding to CH_2 stretching vibrations, – C – C – bending and CF_2 symmetric stretching vibrations[45]. The peak at 1652 cm^{-1} is due to the bond formed between the polymer backbone and LiTFSI.

PAN+PVdF-HFP+Na-ZSM with LiTFSI shows FT-IR peaks at 1045 cm^{-1} corresponding to the C-F symmetric stretching bond of PVdF-HFP. Furthermore, the extra peak at 2247 cm^{-1} is due to the C – N triple bond form the PAN polymer. The FT-IR comparison of PAN+PVdF-HFP+Ti-ZSM showed all the peaks similar to that of the one with Na-ZSM.

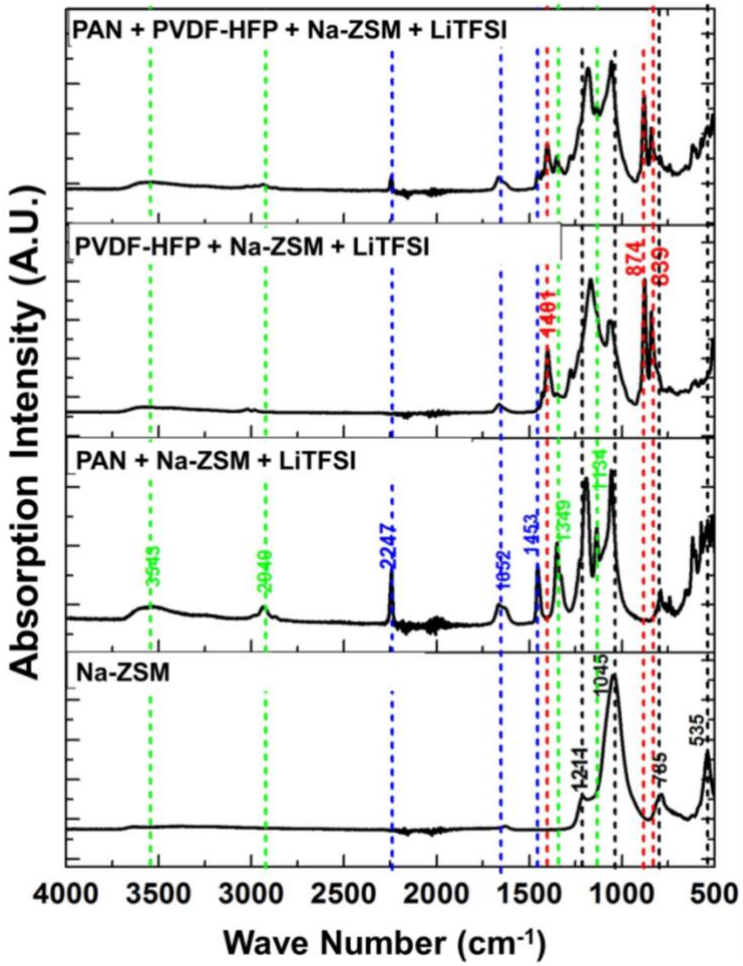

Figure 11. FTIR spectra of commercial Na-ZSM (bottom), PAN + Na-ZSM + LiTFSI (center) and PVdF-HFP + Na-ZSM + LiTFSI, PAN+ PVdF-HFP + Na-ZSM + LiTFS (Top).

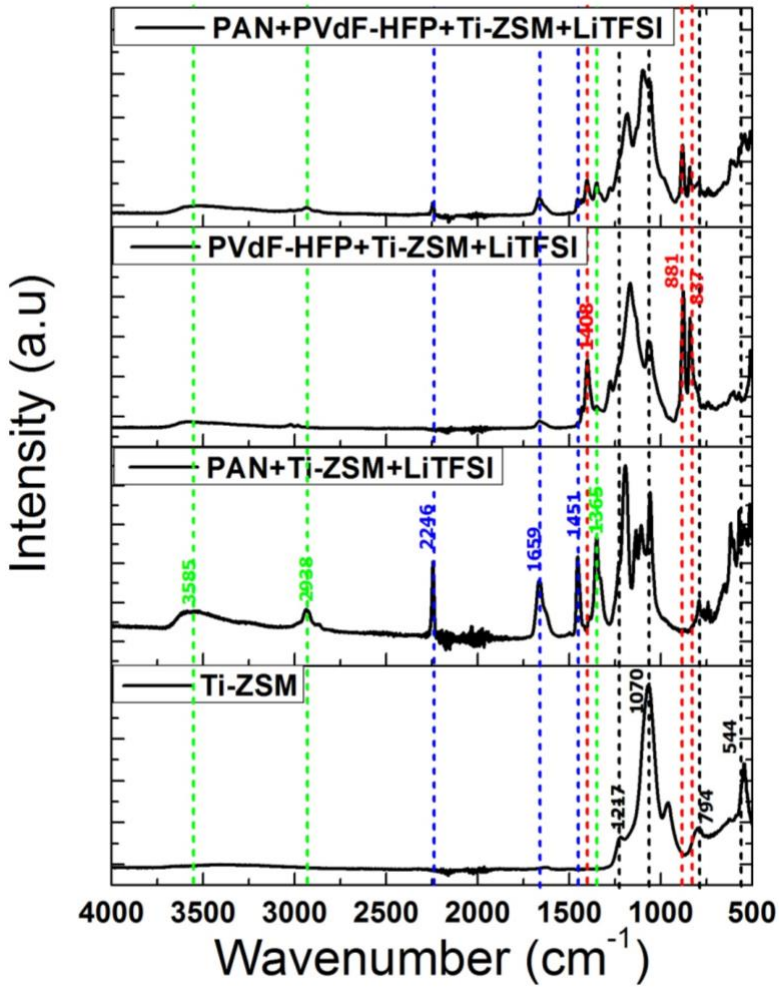

Figure 12. FTIR spectra of commercial Ti-ZSM (bottom), PAN + Ti-ZSM + LiTFSI (center) and PVdF-HFP + Ti-ZSM + LiTFSI, PAN+ PVdF-HFP + Ti-ZSM + LiTFS (Top).

3.2.4 Surface engineering of lithium

Fig. 13 shows the SEM images comparing the morphology of the plane foil and the patterned/imprinted lithium foil. Plain lithium foil shows a smooth surface with minimal defects while surface engineered lithium also shows the ridged pattern replicated from the surface of the commercial filer due to the deformation force of the rolling process. The mechanical deformation energy stored in the trenches during the surface engineering process is expected to create highly active sites inside the trenches and along the walls of these trenches thus, altering the nucleation

and growth mechanism whilst modifying the morphology and nucleation sites for Li plating/ deplating[46].

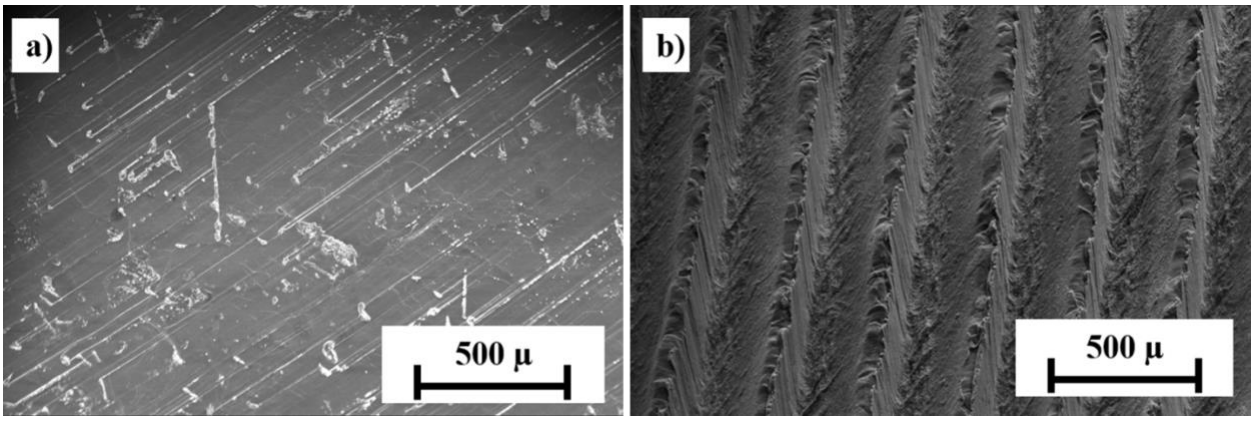

Figure 13. SEM images of a) commerical lithium foil, b) surface engineered lithium foil**.**

3.3 ELECTROCHEMICAL PERFORMANCE

3.3.1 Sulfur infiltrated ZSM

The sulfur infiltrated ZSM-5 were tested in CR2025 coincells using a liquid electrolyte comprising of 1M LiTFSI, 0.2M LiNO3 in DOL:DME (50:50 vol.%) in a potential window of 1.5V – 2.6V at different current rates of 150mA/g the results of which are shown in Fig 14. The normalized specific capacity (n^{th} cycle specific capacity / 1^{st} cycle specific capacity) shown in **Fig. 14a** provides an accurate comparison of the relative cycling performance of two different systems. The initial fade in LiZSM-S obtained after ion exchange with LiCl solution is lower as compared to HZSM-S indicating the improvement in the electrochemical performance of Li-ZSM, probably due to the enhancement in the Li^+ conductivity of the host ZSM. Additionally, in LiZSM-S shows much lower initial capacity loss as well as long term fade rate as observed in the normalized

capacity plots. Commercial sulfur shows an initial capacity of ~750mAh/g with a rapid fade rate due to the formation and dissolution of polysulfides in the electrolyte (**Fig. 14b**). However, by using LiZSM as host material for sulfur the initial capacity is improved to ~950-1150mAh/g along with a decrease in the fade rate by hindering the polysulfide dissolution and transport within the cathode. Further prevention/ reduction of the polysulfide dissolution and shuttling requires replacement of the liquid electrolyte with a hybrid structure combining the properties of liquid electrolyte with celgard separator whilst maintaining the Li+ conductivity close to that of liquid electrolyte.

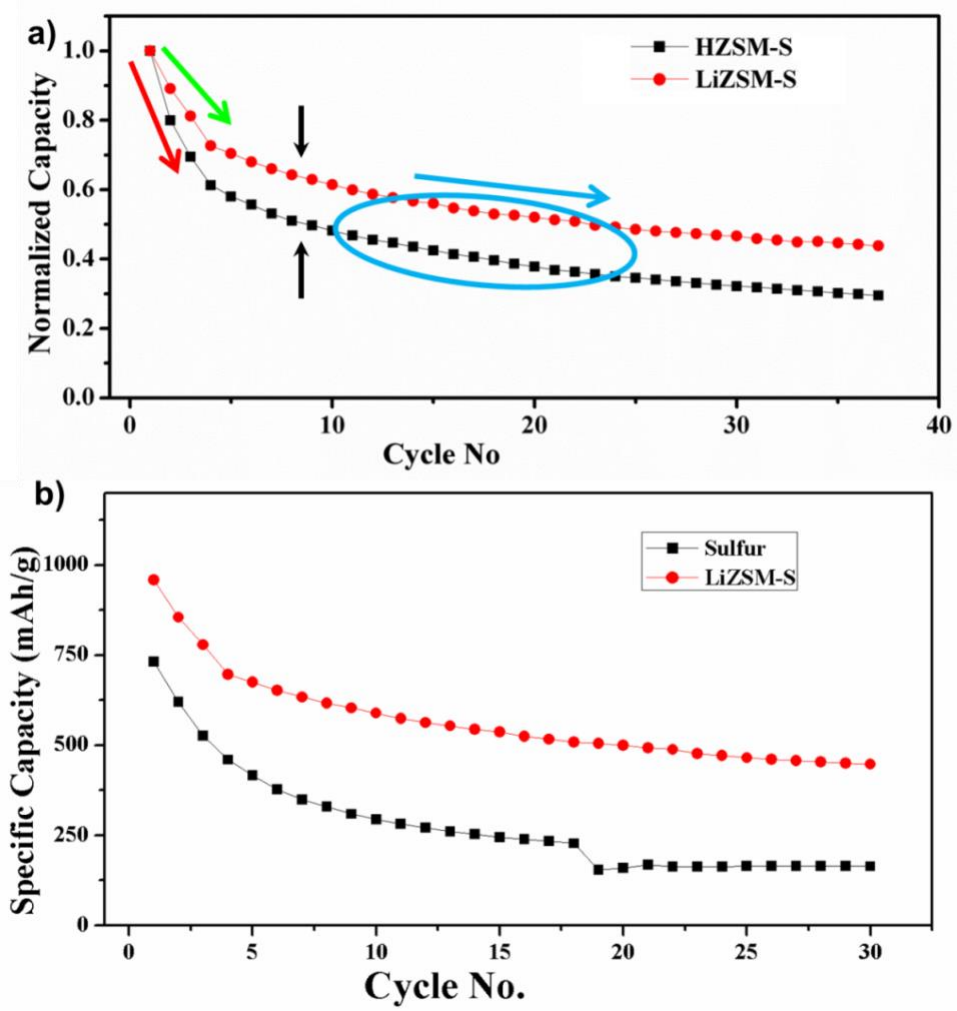

Figure 14. a) Normalized capacity , b) specific capacity plots showing relative cycling behavior of different sulfur infiltrated ZSM and commercial sulfur in liquid electrolyte in Li/Li+ system.

3.3.2 Composite polymer electrolyte, commercial sulfur cathode and lithium metal anode

Composite polymer electrolytes based on PAN, PVDF-HFP polymers along with different ZSM-5 fillers were identified and designed to replace liquid electrolyte and commercial Celgard separator. The electrochemical performances of the CPEs were studied by cycling them with commercial sulfur cathode. The electrochemical cycling performance and coulombic efficiency of the CPE based system with commercial sulfur based cathode is as shown in **Fig. 15**. The PAN/PVdF-HFP-Ti-ZSM composite polymer electrolyte show an initial discharge capacity of

~1038.85 mAh·g^{-1}, columbic efficiency of >99%, a stable capacity of ~691.45 mAh·g^{-1} with a fade rate is ~8.66 mAh·g^{-1} per cycle at the end of 40 cycles. The stable performance of the CPEs indicates that the polysulfide dissolution and shuttling is suppressed by CPEs with Ti-ZSM as filler.

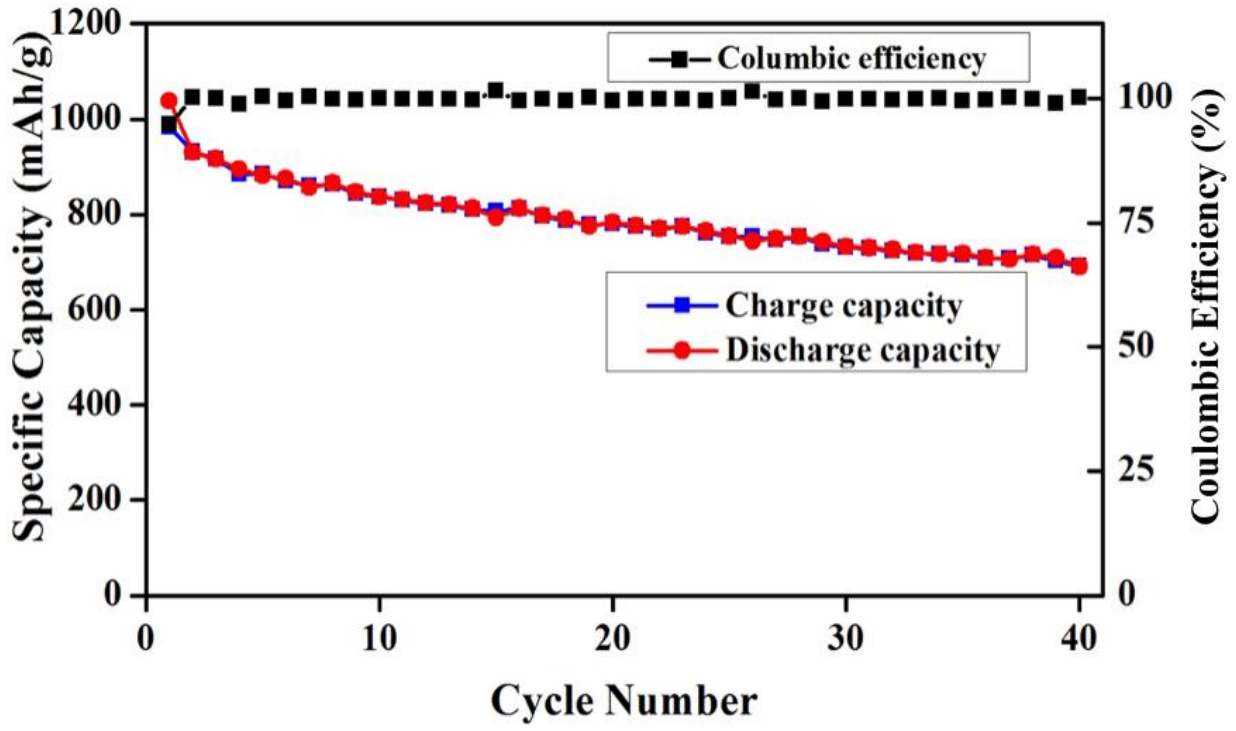

Figure 15. Cycling performance of commercial sulfur cathodes using Ti-ZSM based CPE in Li/Li+ system.

Fig. 16 shows the electrochemical cycling performance of PAN/PVdF-HFP polymer electrolytes with Na-ZSM as filler instead of Ti-ZSM. The Na-ZSM based GPEs show an initial discharge capacity of ~944.74 mAh·g^{-1} and a stable cycling capacity ~671.94 mAh·g^{-1} with a fade of ~6.82 mAh·g^{-1} per cycle at the end of 40 cycles. The columbic efficiency of the system is > 99% and the lower capacity fade of Na-ZSM based CPE confirms efficient suppression of polysulfide dissolution and shuttling as compared to Ti-ZSM based CPE during the electrochemical cycling

performance in Li/Li^+ system. Therefore, adding Na-ZSM filler to the CPEs contributes to improved cycle performance of lithium-sulfur batteries.

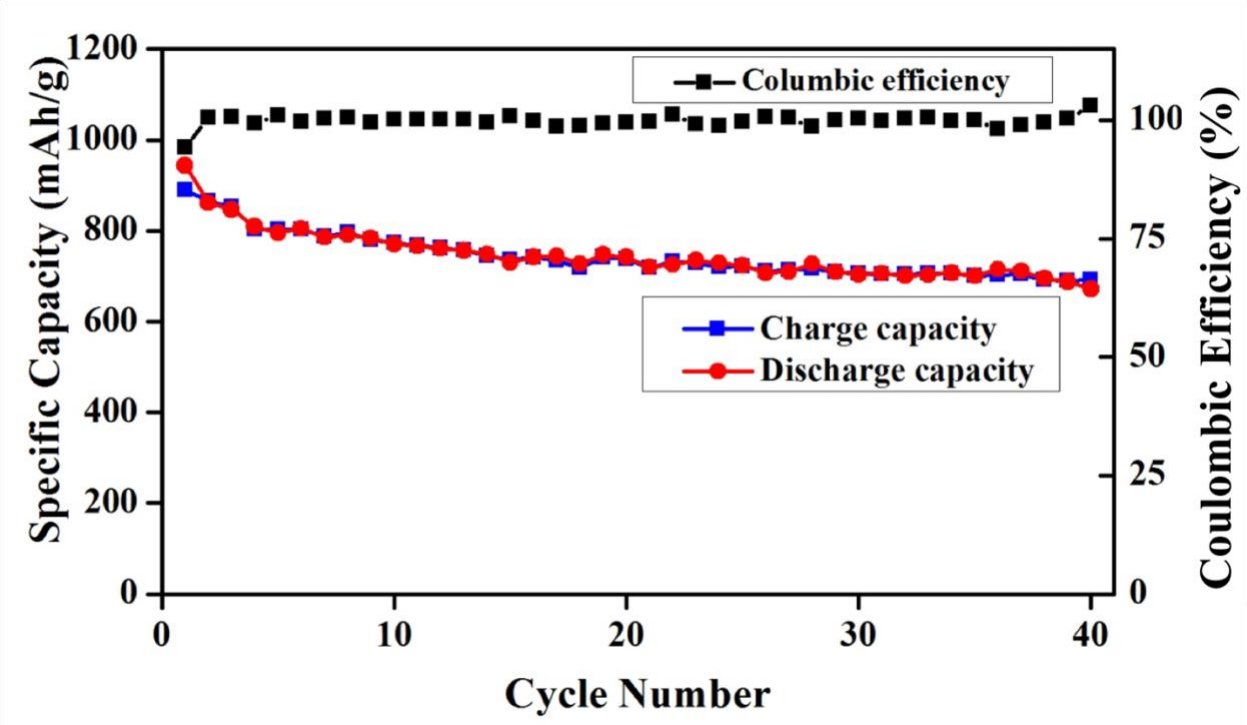

Figure 16. Cycling performance of commercial sulfur cathodes using Ti-ZSM based CPE in Li/Li+ system.

Fig. 17 and **Table 2** represent the comparison of the performance of both the CPEs with commercial sulfur cathodes. It shows that without filler, the CPEs gave initial discharge capacity of 1050.89 $mAh \cdot g^{-1}$ which quickly fade to 335.29 $mAh \cdot g^{-1}$ after 40 cycles with a high fade rate of 17.39 $mAh \cdot g^{-1}$ per cycle due to suspected polysulfide shuttling issue. There is a significant improvement upon using Na-ZSM and Ti-ZSM filler for CPEs due to prevention of polysulfide diffusion, shuttling and dissolution. The Ti-ZSM based CPE shows an initial higher capacity however, suffers from higher fade rate while the Na-ZSM based CPE shows improved electrochemical cycling behavior with lower fade rate between the two CPE systems tested in LIB.

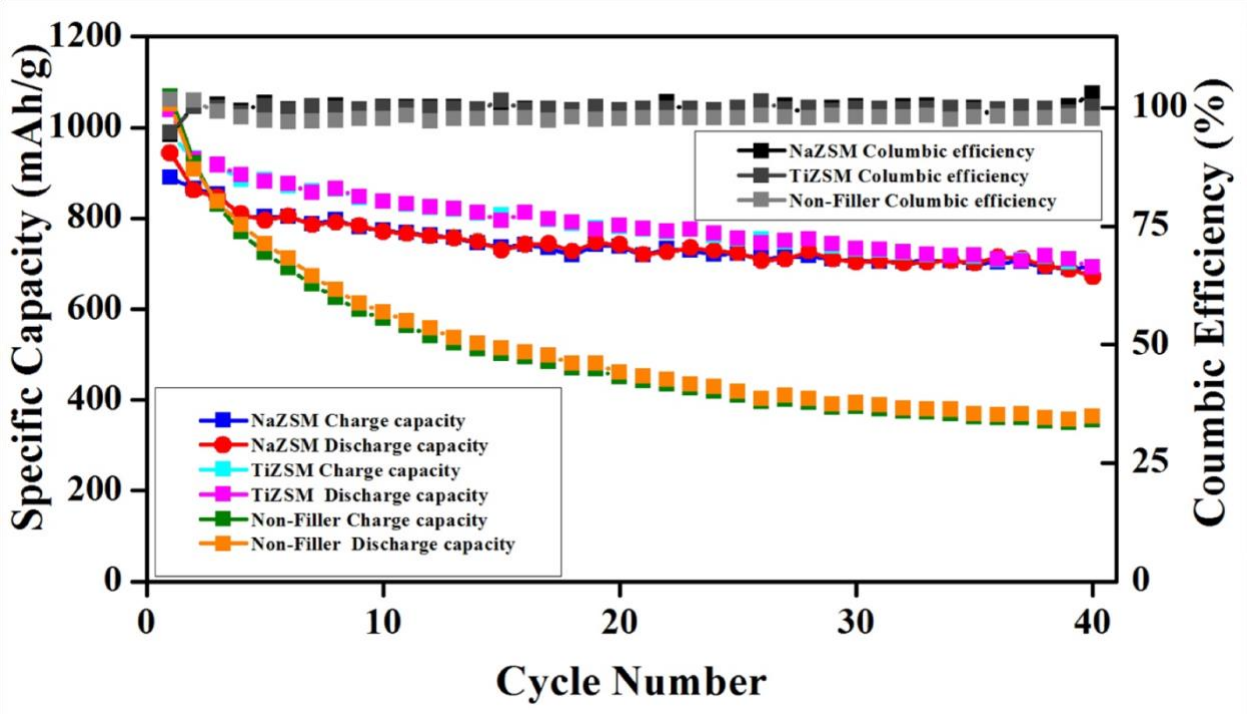

Figure 17. No filler. NaZSM, TiZSM with commerical sulfur and Li foil.

Table 2. The comparison of different types fillers of CPEs including: Ti-ZSM, Na-ZSM and non-filler.

Electrolyte	Initial Discharge Capacity/ mAh·g^{-1}	Fade Rate/ mAh·g^{-1}/cycle
Ti-ZSM-GPE	1037.85	8.66
Na-ZSM-GPE	944.74	6.82
Non-filler GPE	1050.89	17.36

3.3.3 ZSM-S cathode, NaZSM- CPE and Surface engineered lithium anode

LiZSM-S as cathode system shows improved performance as compared to commercial sulfur cathodes, while NaZSM based CPE membranes show stable cycling behavior as compared to liquid electrolyte based systems. Hyun et. al. have showed improved lithium plating/deplating

process with the delayed growth of mossy and dendritic Li and reduction of SEI layer due to the formation of high surface area Li on the surface of anode. Hence, to further improve the cycling performance high performing LiZSM-S cathode system was integrated with Na-ZSM based CPE membrane and surface engineered Li as anode system and the electrochemical performance of this integrated system was studied in LIB. The combination of GPEs and LiZSM-S provides the advantage of increased active material utilization in addition to restraining the polysulfide dissolution/shuttling. **Fig. 18a and 18b** represents the electrochemical performance of PVdF-HFP+PAN-ZSM system at different current rates. The results of LiZSM-S cathode cycled at 50 $mA \cdot g^{-1}$ current is represented in the **Fig. 17a**, exhibits an initial discharge capacity of 920.91 $mAh \cdot g^{-1}$ without any first cycle irreversible loss, a stable capacity of 887.61 $mAh \cdot g^{-1}$ and a very low fade rate of ~3.33 $mAh \cdot g^{-1}$ per cycle at the end of 10^{th} cycle when tested at C/14 charge/discharge rate. Subsequently, the the system was subjected to higher current rate of 100 $mA \cdot g^{-1}$ (**Fig. 18b)** to check for the electrochemical stability and performance of the system under increased Li+ flux between the cathode and anode. The system exhibited an initial discharge capacity of ~912 $mAh \cdot g^{-1}$, no major irreversible loss and a stable capacity of ~782.50 $mAh \cdot g^{-1}$ with a minimal fade rate of 5.18 $mAh \cdot g^{-1}$ at the end of 25^{th} cycle which is a considerable improvement in the performance of Li – S battery when compared to commercial sulfur based cathodes and liquid based electrolytes.

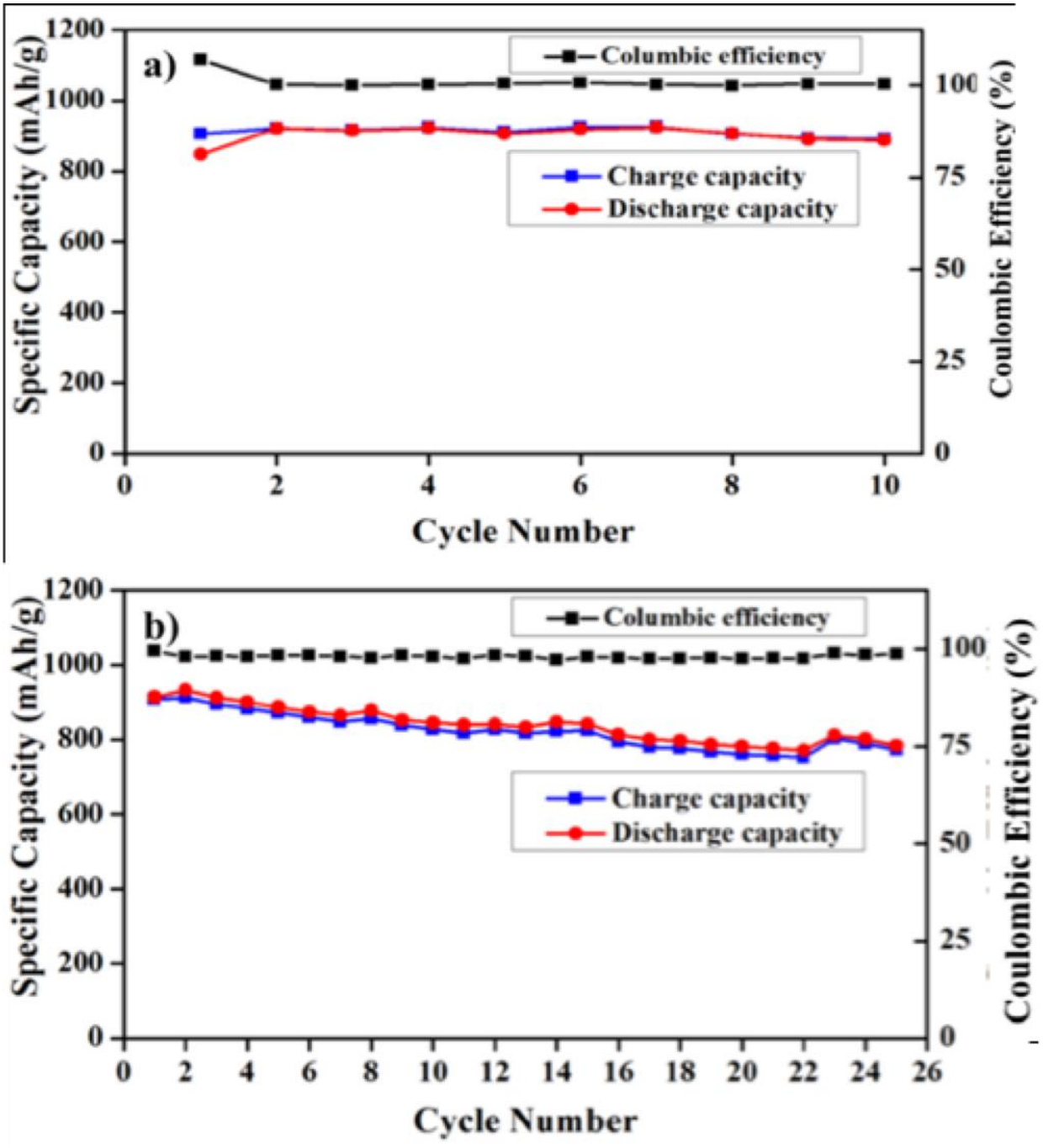

Figure 18. NaZSM with LiZSM-S and SE-Li foil a) C/14, b) C/8 rates.

4.0 CONCLUSIONS

In this research conducted over the past one year, Na-ZSM and Ti-ZSM incorporated CPEs were synthesized by electrospinning PAN and PVdF-HFP polymers and tested as the electrolyte/separator in lithium-sulfur battery. The BET surface area analysis confirmed the high surface area of Na-ZSM and Ti-ZSM. These nanofiller incorporated electrospun CPEs improved the electrochemical performance of lithium-sulfur battery. With the commercial sulfur cathodes, the Na-ZSM CPEs exhibited an initial discharge of 944.74 $mAh \cdot g^{-1}$ and a relatively low fade rate of 6.82 $mAh \cdot g^{-1}$cycle when cycled at 100 mA h^{-1}. Compared to the electrochemical performance of CPEs, the nano-filler incorporated CPEs shows better performance due to their ability to prevent the polysulfide dissolution in electrolyte and shuttling between the two electrodes. In comparison with commercial sulfur cathode, the Li^{+} substituted sulfur infiltrated HZSM-5 (LiZSM-S) cathode showed improved electrochemical cycling performance in LIB system due to the likely entrapment of polysulfide species in the highly porous structure of ZSM-5 which hinders polysulfide diffusion at the cathode – electrolyte interface. The performance of the Na-ZSM based CPE was also tested by integrating it with LiZSM-S as cathode system and surface engineered lithium as anode system. An initial discharge capacity of ~920.91 $mAh \cdot g^{-1}$ with a very low fade rate of ~3.33 $mAh \cdot g^{-1}$ per cycle at the end of 10 cycles was observed in the integrated system when tested at a current rate of 50 mA g^{-1}. At 100 mA g^{-1} rate, a stable performance was maintained with an initial discharge capacity of 912 $mAh \cdot g^{-1}$ and fade rate of ~5.18 $mAh \cdot g^{-1}$ per cycle at the end of 25 cycles. These initial results show the promise of using Na-ZSM based nanofillers in PAN-PVdf-HFP CPEs as

well as ion-exchanged LiZSM cathodes combined with surface engineered Li metal anodes. Further detailed work is clearly warranted to understand the mechanisms contributing to the promising initial results observed and reported in this Master of Science thesis research. These studies will be planned in the near future.

BIBLIOGRAPHY

1. Epur, R.; Datta, M. K.; Kumta, P. N., Nanoscale engineered electrochemically active silicon-CNT heterostructures-novel anodes for Li-ion application. *Electrochim Acta* **2012,** *85*, 680-684.

2. Winter, M.; Brodd, R. J., What are batteries, fuel cells, and supercapacitors? *Chemical Reviews* **2004,** *104* (10), 4245-4269.

3. Mizushima, K.; Jones, P. C.; Wiseman, P. J.; Goodenough, J. B., Lixcoo2 (O Less-Than X Less-Than-or-Equal-to 1) - a New Cathode Material for Batteries of High-Energy Density. *Solid State Ionics* **1981,** *3-4* (Aug), 171-174.

4. Tran, T. D.; Feikert, J. H.; Song, X.; Kinoshita, K., Commercial Carbonaceous Materials as Lithium Intercalation Anodes. *J Electrochem Soc* **1995,** *142* (10), 3297-3302.

5. Weydanz, W. J.; Wohlfahrt-Mehrens, M.; Huggins, R. A., A room temperature study of the binary lithium–silicon and the ternary lithium–chromium–silicon system for use in rechargeable lithium batteries. *J Power Sources* **1999,** *81-82*, 237-242.

6. Tarascon, J. M.; Armand, M., Issues and challenges facing rechargeable lithium batteries. *Nature* **2001,** *414* (6861), 359-367.

7. CHAN, C. K.; PENG, H.; LIU, G.; McILWRATH, K.; ZHANG, X. F.; HUGGINS, R. A.; CUI, Y., High-performance lithium battery anodes using silicon nanowires. In *Materials for Sustainable Energy*, pp 187-191.

8. Park, M.-H.; Kim, M. G.; Joo, J.; Kim, K.; Kim, J.; Ahn, S.; Cui, Y.; Cho, J., Silicon Nanotube Battery Anodes. *Nano Letters* **2009,** *9* (11), 3844-3847.

9. Mizushima, K.; Jones, P. C.; Wiseman, P. J.; Goodenough, J. B., Lixcoo2 "(Oless-Thanxless-Than-or-Equal-To1) - a New Cathode Material for Batteries of High-Energy Density. *Mater Res Bull* **1980,** *15* (6), 783-789.

10. Wang, D. W.; Zeng, Q. C.; Zhou, G. M.; Yin, L. C.; Li, F.; Cheng, H. M.; Gentle, I. R.; Lu, G. Q. M., Carbon-sulfur composites for Li-S batteries: status and prospects. *J Mater Chem A* **2013,** *1* (33), 9382-9394.

11. Kolosnitsyn, V. S.; Karaseva, E. V., Lithium-sulfur batteries: Problems and solutions. *Russ J Electrochem+* **2008,** *44* (5), 506-509.

12. Jeon, B. H.; Yeon, J. H.; Chung, I. J., Preparation and electrical properties of lithium–sulfur-composite polymer batteries. *Journal of Materials Processing Technology* **2003,** *143-144*, 93-97.

13. Bruce, P. G.; Freunberger, S. A.; Hardwick, L. J.; Tarascon, J. M., Li-O-2 and Li-S batteries with high energy storage (vol 11, pg 19, 2012). *Nat Mater* **2012,** *11* (2).

14. Manthiram, A.; Fu, Y.; Chung, S.-H.; Zu, C.; Su, Y.-S., Rechargeable Lithium–Sulfur Batteries. *Chemical Reviews* **2014,** *114* (23), 11751-11787.

15. Zeng, P.; Huang, L. W.; Zhang, X. L.; Zhang, R. X.; Wu, L.; Chen, Y. G., Long-life and high-areal-capacity lithium-sulfur batteries realized by a honeycomb-like N, P dual-doped carbon modified separator. *Chem Eng J* **2018,** *349*, 327-337.

16. Fu, C. Y.; Guo, J. C., Challenges and current development of sulfur cathode in lithium-sulfur battery. *Curr Opin Chem Eng* **2016,** *13*, 53-62.

17. Manthiram, A.; Fu, Y. Z.; Su, Y. S., Challenges and Prospects of Lithium-Sulfur Batteries. *Accounts Chem Res* **2013,** *46* (5), 1125-1134.

18. Lv, D. P.; Zheng, J. M.; Li, Q. Y.; Xie, X.; Ferrara, S.; Nie, Z. M.; Mehdi, L. B.; Browning, N. D.; Zhang, J. G.; Graff, G. L.; Liu, J.; Xiao, J., High Energy Density Lithium-Sulfur Batteries: Challenges of Thick Sulfur Cathodes. *Adv Energy Mater* **2015,** *5* (16).

19. Zhang, B.; Qin, X.; Li, G. R.; Gao, X. P., Enhancement of long stability of sulfur cathode by encapsulating sulfur into micropores of carbon spheres. *Energ Environ Sci* **2010,** *3* (10), 1531-1537.

20. Yuan, L.; Yuan, H.; Qiu, X.; Chen, L.; Zhu, W., Improvement of cycle property of sulfur-coated multi-walled carbon nanotubes composite cathode for lithium/sulfur batteries. *J Power Sources* **2009,** *189* (2), 1141-1146.

21. Zheng, W.; Liu, Y. W.; Hu, X. G.; Zhang, C. F., Novel nanosized adsorbing sulfur composite cathode materials for the advanced secondary lithium batteries. *Electrochim Acta* **2006,** *51* (7), 1330-1335.

22. Yuan, L. X.; Feng, J. K.; Ai, X. P.; Cao, Y. L.; Chen, S. L.; Yang, H. X., Improved dischargeability and reversibility of sulfur cathode in a novel ionic liquid electrolyte. *Electrochemistry Communications* **2006,** *8* (4), 610-614.

23. J., W.; J., Y.; J., X.; N., X., A Novel Conductive Polymer–Sulfur Composite Cathode Material for Rechargeable Lithium Batteries. *Advanced Materials* **2002,** *14* (13‐14), 963-965.

24. Yin, L.; Wang, J.; Lin, F.; Yang, J.; Nuli, Y., Polyacrylonitrile/graphene composite as a precursor to a sulfur-based cathode material for high-rate rechargeable Li–S batteries. *Energ Environ Sci* **2012,** *5* (5), 6966-6972.

25. Wang, J.; Chen, J.; Konstantinov, K.; Zhao, L.; Ng, S. H.; Wang, G. X.; Guo, Z. P.; Liu, H. K., Sulphur-polypyrrole composite positive electrode materials for rechargeable lithium batteries. *Electrochim Acta* **2006,** *51* (22), 4634-4638.

26. J., W.; J., Y.; C., W.; K., D.; J., X.; N., X., Sulfur Composite Cathode Materials for Rechargeable Lithium Batteries. *Advanced Functional Materials* **2003,** *13* (6), 487-492.

27. Xiao, L.; Yuen, K. C.; Fernanda, L.-M.; Quan, P.; Marine, C.; He, H.; J., H. C.; Diane, H.; Kavish, K.; Heino, S.; Torsten, B.; Jürgen, J.; F., N. L., Tuning Transition Metal Oxide–Sulfur Interactions for Long Life Lithium Sulfur Batteries: The "Goldilocks" Principle. *Adv Energy Mater* **2016,** *6* (6), 1501636.

28. Tao, X.; Wang, J.; Liu, C.; Wang, H.; Yao, H.; Zheng, G.; Seh, Z. W.; Cai, Q.; Li, W.; Zhou, G.; Zu, C.; Cui, Y., Balancing surface adsorption and diffusion of lithium-polysulfides on nonconductive oxides for lithium–sulfur battery design. *Nature Communications* **2016,** *7*, 11203.

29. Liang, C. D.; Dudney, N. J.; Howe, J. Y., Hierarchically Structured Sulfur/Carbon Nanocomposite Material for High-Energy Lithium Battery. *Chem Mater* **2009,** *21* (19), 4724-4730.

30. Xin, S.; Guo, Y.-G.; Wan, L.-J., Nanocarbon Networks for Advanced Rechargeable Lithium Batteries. *Accounts Chem Res* **2012,** *45* (10), 1759-1769.

31. Jin, J.; Wen, Z.; Ma, G.; Lu, Y.; Rui, K., Mesoporous carbon/sulfur composite with polyaniline coating for lithium sulfur batteries. *Solid State Ionics* **2014,** *262*, 170-173.

32. Shanthi, P. M.; Hanumantha, P. J.; Gattu, B.; Sweeney, M.; Datta, M. K.; Kumta, P. N., Understanding the Origin of Irreversible Capacity loss in Non-Carbonized Carbonate − based Metal Organic Framework (MOF) Sulfur hosts for Lithium − Sulfur battery. *Electrochim Acta* **2017,** *229*, 208-218.

33. Junghoon, K.; Dong-Ju, L.; Hun-Gi, J.; Yang-Kook, S.; Jusef, H.; Bruno, S., An Advanced Lithium-Sulfur Battery. *Advanced Functional Materials* **2013,** *23* (8), 1076-1080.

34. Shim, J.; Striebel, K. A.; Cairns, E. J., The Lithium/Sulfur Rechargeable Cell: Effects of Electrode Composition and Solvent on Cell Performance. *Journal of The Electrochemical Society* **2002,** *149* (10), A1321-A1325.

35. Shin, J. H.; Kim, K. W.; Ahn, H. J.; Ahn, J. H., Electrochemical properties and interfacial stability of (PEO)10LiCF3SO3–TinO2n−1 composite polymer electrolytes for lithium/sulfur battery. *Materials Science and Engineering: B* **2002,** *95* (2), 148-156.

36. Hassoun, J.; Scrosati, B., Moving to a Solid-State Configuration: A Valid Approach to Making Lithium-Sulfur Batteries Viable for Practical Applications. *Advanced Materials* **2010,** *22* (45), 5198-5201.

37. Liang, X.; Wen, Z.; Liu, Y.; Zhang, H.; Huang, L.; Jin, J., Highly dispersed sulfur in ordered mesoporous carbon sphere as a composite cathode for rechargeable polymer Li/S battery. *Journal of Power Sources* **2011,** *196* (7), 3655-3658.

38. Dai, C.; Zhang, A.; Liu, M.; Guo, X.; Song, C., Hollow ZSM-5 with Silicon-Rich Surface, Double Shells, and Functionalized Interior with Metallic Nanoparticles and Carbon Nanotubes. *Advanced Functional Materials* **2015,** *25* (48), 7479-7487.

39. Zhang, X.; Liu, D.; Xu, D.; Asahina, S.; Cychosz, K. A.; Agrawal, K. V.; Al Wahedi, Y.; Bhan, A.; Al Hashimi, S.; Terasaki, O.; Thommes, M.; Tsapatsis, M., Synthesis of Self-Pillared Zeolite Nanosheets by Repetitive Branching. *Science* **2012,** *336* (6089), 1684-1687.

40. Kumar, B.; Scanlon, L. G., Polymer-ceramic composite electrolytes. *J Power Sources* **1994,** *52* (2), 261-268.

41. Majano, G.; Darwiche, A.; Mintova, S.; Valtchev, V., Seed-Induced Crystallization of Nanosized Na-ZSM-5 Crystals. *Industrial & Engineering Chemistry Research* **2009,** *48* (15), 7084-7091.

42. Mohamed, R. M.; Ismail, A. A.; Othman, I.; Ibrahim, I. A., Preparation of TiO2-ZSM-5 zeolite for photodegradation of EDTA. *J Mol Catal a-Chem* **2005,** *238* (1-2), 151-157.

43. Jung, K. N.; Lee, J. I.; Jung, J. H.; Shin, K. H.; Lee, J. W., A quasi-solid-state rechargeable lithium-oxygen battery based on a gel polymer electrolyte with an ionic liquid. *Chemical Communications* **2014,** *50* (41), 5458-5461.

44. Caldeira, V. P. S.; Santos, A. G. D.; Pergher, S. B. C.; Costa, M. J. F.; Araujo, A. S., USE OF A LOW-COST TEMPLATE-FREE ZSM-5 FOR ATMOSPHERIC PETROLEUM RESIDUE PYROLYSIS. *Química Nova* **2016,** *39*, 292-297.

45. M. Shanthi, P.; J. Hanumantha, P.; Albuquerque, T.; Gattu, B.; Kumta, P. N., Novel Composite Polymer Electrolytes of PVdF-HFP Derived by Electrospinning with Enhanced Li-Ion Conductivities for Rechargeable Lithium–Sulfur Batteries. *ACS Applied Energy Materials* **2018,** *1* (2), 483-494.

46. Myung-Hyun, R.; Min, L. Y.; Yunju, L.; Martin, W.; Peter, B., Mechanical Surface Modification of Lithium Metal: Towards Improved Li Metal Anode Performance by Directed Li Plating. *Advanced Functional Materials* **2015,** *25* (6), 834-841.